

## Article

# Magnetic Bead Handling Using a Paper-Based Device for Quantitative Point-of-Care Testing

Kevin Arias-Alpizar<sup>1,2</sup>, Ana Sánchez-Cano<sup>1,2</sup>, Judit Prat-Trunas<sup>1</sup>, Elena Sulleiro<sup>2,3,4</sup> , Pau Bosch-Nicolau<sup>3,4</sup> , Fernando Salvador<sup>3,4</sup>, Inés Oliveira<sup>3,4</sup>, Israel Molina<sup>3,4</sup>, Adrián Sánchez-Montalvá<sup>2,3,4</sup> and Eva Baldrich<sup>1,4,\*</sup> 

<sup>1</sup> Diagnostic Nanotools Group, Vall d'Hebron Institut de Recerca (VHIR), 08035 Barcelona, Spain

<sup>2</sup> Universitat Autònoma de Barcelona (UAB), 08193 Barcelona, Spain

<sup>3</sup> International Health Unit Vall d'Hebron-Drassanes, Vall d'Hebron Hospital Universitari, PROSICS Barcelona, 08035 Barcelona, Spain

<sup>4</sup> Centro de Investigación Biomédica en Red de Enfermedades Infecciosas (CIBERINFEC), Instituto de Salud Carlos III, 28028 Madrid, Spain

\* Correspondence: eva.baldrich@vhir.org

**Abstract:** Microfluidic paper-based analytical devices ( $\mu$ PADs) have been extensively proposed as ideal tools for point-of-care (POC) testing with minimal user training and technical requirements. However, most  $\mu$ PADs use dried bioreagents, which complicate production, reduce device reproducibility and stability, and require transport and storage under temperature and humidity-controlled conditions. In this work, we propose a  $\mu$ PAD produced using an affordable craft-cutter and stored at room temperature, which is used to partially automate a single-step colorimetric magneto-immunoassay. As a proof-of-concept, the  $\mu$ PAD has been applied to the quantitative detection of *Plasmodium falciparum* lactate dehydrogenase (Pf-LDH), a biomarker of malaria infection. In this system, detection is based on a single-step magneto-immunoassay that consists of a single 5-min incubation of the lysed blood sample with immuno-modified magnetic beads (MB), detection antibody, and an enzymatic signal amplifier (Poly-HRP). This mixture is then transferred to a single-piece paper device where, after on-chip MB magnetic concentration and washing, signal generation is achieved by adding a chromogenic enzyme substrate. The colorimetric readout is achieved by the naked eye or using a smartphone camera and free software for image analysis. This  $\mu$ PAD afforded quantitative Pf-LDH detection in <15 min, with a detection limit of  $6.25 \text{ ng mL}^{-1}$  when the result was interpreted by the naked eye and  $1.4 \text{ ng mL}^{-1}$  when analysed using the smartphone imaging system. Moreover, the study of a battery of clinical samples revealed concentrations of Pf-LDH that correlated with those provided by the reference ELISA and with better sensitivity than a commercial rapid diagnostic test (RDT). These results demonstrate that magneto-immunoassays can be partly automated by employing a  $\mu$ PAD, achieving a level of handling that approaches the requirements of POC testing.

**Keywords:** immuno-modified magnetic beads; paper-based diagnostic device; low-cost assay automation; smartphone colorimetric detection; point-of-care testing; malaria quantitative diagnosis



**Citation:** Arias-Alpizar, K.; Sánchez-Cano, A.; Prat-Trunas, J.; Sulleiro, E.; Bosch-Nicolau, P.; Salvador, F.; Oliveira, I.; Molina, I.; Sánchez-Montalvá, A.; Baldrich, E. Magnetic Bead Handling Using a Paper-Based Device for Quantitative Point-of-Care Testing. *Biosensors* **2022**, *12*, 680. <https://doi.org/10.3390/bios12090680>

Received: 26 July 2022

Accepted: 20 August 2022

Published: 25 August 2022

**Publisher's Note:** MDPI stays neutral with regard to jurisdictional claims in published maps and institutional affiliations.



**Copyright:** © 2022 by the authors. Licensee MDPI, Basel, Switzerland. This article is an open access article distributed under the terms and conditions of the Creative Commons Attribution (CC BY) license (<https://creativecommons.org/licenses/by/4.0/>).

## 1. Introduction

Paper and paper-like materials are extensively employed to produce analytical tools [1,2]. Compared to other alternatives, such as glass-, silicon- or polymer-based chips,  $\mu$ PADs are inexpensive, relatively easy to fabricate, and convenient to dispose of. The porous membrane provides filtration and pre-treatment of complex samples, large surface areas for reagent incorporation, and passive solution pumping without external power sources or equipment. When coupled to the visual interpretation of a colorimetric readout,  $\mu$ PADs approach ideal POC diagnostic devices, matching the ASSURED criteria established by the World Health Organization (WHO): affordable, sensitive, specific, user-friendly, rapid and robust, equipment free, and deliverable to end-users [3].

The most widely used  $\mu$ PADs are lateral-flow assays (LFAs), which consist of 4 types of overlapping membranes (sample, conjugate, test and absorbent pads, respectively), two of them containing dried reagents [4]. To carry a test, the user dispenses the sample (and sometimes running buffer), which wicks along the device to interact with a labelled detection antibody (d-Ab) and the immobilized capture antibody (c-Ab), forming coloured bands that are interpreted visually or using hand-held readers [5]. More sophisticated  $\mu$ PADs incorporate hydrophobic barriers to define hydrophilic channels and chambers (such as by paper patterning, multi-component stacking, or folding into three-dimensional origami chips) [1,2]. When reagent-modified,  $\mu$ PADs display limited stability and should be distributed and stored under controlled temperature and humidity [2]. In addition, reagent-modified  $\mu$ PADs can be used only to detect the analyte they were produced for.

Malaria is a disease caused by *Plasmodium* parasites that are transmitted to humans by the bite of infected female *Anopheles* mosquitoes [6]. Despite being curable, malaria took the life of 627,000 people and caused 241 million cases in 2020 [7]. Of the human-infecting *Plasmodium* species, *P. falciparum* is the most frequent and deadly, accounting for 94% of the cases and deaths reported worldwide. There is a general agreement that factors such as increasing parasite drug resistance [8], migration processes [9], climate change effects [10], growth of the population at risk, and the COVID-19 pandemic [8] combine to jeopardise the advances made over the last decades to control the disease in the endemic countries, increasing the risk of malaria reintroduction in areas from which it had been eliminated.

Currently, the “gold standard” for the diagnosis of malaria is microscopy [11,12]. Although a well-trained microscopist can detect down to 50–100 parasites per  $\mu$ L of blood (parasite  $\mu\text{L}^{-1}$ ) under typical field conditions [13], microscopy relies on expertise and subjective result interpretation, requires >1 h per sample, and cannot detect low parasitemias (so-called submicroscopic malaria). In centralised laboratories, molecular techniques, such as the polymerase chain reaction (PCR), are gradually being incorporated, achieving exceptional LODs (around 1 parasite  $\mu\text{L}^{-1}$ ), often in fully automated and species-specific assay formats. However, PCR demands long analysis time, experienced personnel, sophisticated infrastructure and high operational costs. Finally, RDTs have been positioned as fast, inexpensive, and easy-to-use tools for malaria POC testing in low/middle-resource settings (such as the countries where malaria is more prevalent) or as the first test in high-resource non-endemic settings before performing confirmatory analysis [14–16]. Most RDTs are LFA-based devices that detect *Plasmodium* antigens in a drop of blood, in <30 min, at a cost of 1–5 € [17]. Nonetheless, RDTs display limitations as well, including variable performance depending on the storage and environmental conditions, subjective result interpretation, qualitative (yes/no) response, insufficient sensitivity, and limited detection of “non-*falciparum*” species [18,19].

Attempts have been made to produce upgraded  $\mu$ PADs. For instance, Pilon dos Santos et al. produced a  $\mu$ PAD to detect *P. falciparum* histidine-rich protein 2 (Pf-HRP2) [20]. The paper chip, cut using a  $\text{CO}_2$  laser plotter, displayed 3 discrete areas separated by narrow microfluidic channels. The first served for the addition of sample and peroxidase-labelled d-Ab; the second displayed immobilised c-Ab; and the third granted solution pumping and waste storage. The system displayed an LOD of 4.5–5.0 ng  $\text{mL}^{-1}$  of Pf-HRP2 in saline solution (equivalent to 59–65 parasites  $\mu\text{L}^{-1}$ ) but was not tested in clinical samples. Since Pf-HRP2 is only present in *P. falciparum* and deletions in the *pfhrp2/3* genes may prevent detection by HRP2-based RDTs, alternative Pan *Plasmodium* biomarkers have been targeted [21–24]. A multiplexed  $\mu$ PADs was produced by Deraney and co-workers by stacking 8 layers of wax-patterned paper, two of them modified with gold-labelled d-Ab and immobilised c-Ab [25]. The device detected Pf-HRP2 and Pan *Plasmodium* lactate dehydrogenase (pLDH) in about 20 min, with LODs of 20.3 ng  $\text{mL}^{-1}$  and 80.2 ng  $\text{mL}^{-1}$ , respectively, and achieved detection in spiked lysed blood. Singh et al. employed aptamer-coated MB to trap pLDH and *P. falciparum* glutamate dehydrogenase (Pf-GDH), which were then incubated in a chromogenic enzyme substrate solution [26]. The supernatant was next transferred to a piece of chemically modified chromatographic paper for colour inter-

pretation by the naked eye (qualitative) or using image analysis (quantitative), achieving LODs down to 68–69 pM in spiked serum in about 95 min (equivalent to 2.3–2.4 ng mL<sup>-1</sup>). The electrochemical  $\mu$ PAD reported by Ruiz-Vega and co-workers included a sample filtration unit, a double-sided screen-printed paper electrode and absorbent pads in a low-cost magnetic holder [27]. The system facilitated the partial automation of a single-step magneto-immunoassay and detected Pf-LDH in lysed whole blood. Pf-LDH quantitation was afforded down to 2.47 ng mL<sup>-1</sup> in about 20 min, identifying patients presenting malaria parasitemias > 0.3%.

Here, we develop a  $\mu$ PAD for magneto-immunoassay POC operation. As a proof-of-concept, we report the fast and quantitative detection of Pf-LDH based on a single-step magneto-immunoassay, a generic single-piece microfluidic paper device and smartphone-based colorimetry. The system affords quantitative Pf-LDH detection in lysed whole blood samples in <20 min, with an LOD of 1.4 ng mL<sup>-1</sup> and minor user intervention. However, the storage-stable paper device could be employed to detect other analytes by just adjusting the magneto-immunoassay reagents.

## 2. Material and Methods

### 2.1. Reagents and Biocomponents

Recombinant Pf-LDH was provided by CTK Biotech (San Diego, CA, USA). Monoclonal capture and detection antibodies to pLDH (C01834M and C01835M, c-MAb and d-MAb, respectively) were from Meridian Bioscience (Memphis, TE, USA). The latter were modified with biotin to produce biotinylated d-MAb (bd-MAb; Supporting Information). Carboxylic acid MB of 1  $\mu$ m diameter (Dynabeads MyOne, Invitrogen Ref. 65011 and SpeedBead Magnetic Carboxylate, GEHealthcare Ref. 45152105050250), Streptavidin PolyHRP (Ref. 21140), sulphuric acid 1 M and 1-ethyl-3-(3-dimethylaminopropyl) carbodiimide hydrochloride (EDC) were from Thermo Fisher Scientific (Barcelona, Spain). Bovine serum albumin (BSA), Triton X-100, Tween 20, 3,3',5,5'-Tetramethylbenzidine Liquid Substrate System (TMB; Ref. T0440), and 2-(N-morpholino)ethanesulfonic acid hydrate (MES) were from Sigma-Aldrich (Madrid, Spain). Phosphate-buffered saline tablets (PBS; Barcelona, Spain) produced KH<sub>2</sub>PO<sub>4</sub> 250 mM sodium phosphate, NaCl 150 mM, and KCl 2.7 mM, pH 7.4. Reagent Diluent (10  $\times$  RD, Ref. DY995; equivalent to 10  $\times$  PBS, 10% BSA) was from R&D (Abingdon, UK). The membranes used for device production were Standard 17 and CF5 (Refs. 17114594 and 29008181; Cytiva Europe, Freiburg, Germany). For washing, PBS was supplemented with 0.05% of Tween 20 (PBS-T). Unless otherwise stated, blocking and incubation steps were carried out with PBS supplemented with BSA 1% and 0.05% of Tween 20 (PBST-BSA).

### 2.2. Device Fabrication

The system for partial magneto-immunoassay operation and detection automation included two components, a disposable  $\mu$ PAD and a reusable magnetic holder, which were assembled as previously described in [28] (Figure 1a). Briefly, the main body of the  $\mu$ PAD was a single-piece device, which was designed using Silhouette Studio version 4.4.476 and cut on Standard 17 using an inexpensive craft plotter, Silhouette Cameo 3 (Silhouette America, Lehi, UT, USA; Figure 1b,c). It contained three distinguishable sections (Figure 1b). The first one was a tear-shaped washing pad (23 mm  $\times$  13.5 mm) for the addition of sample and assay reagents. Accordingly, this section was designed to display high-volume load capacity and efficient solution flow towards the second section. This was an MB concentration zone 5 mm in diameter, which was placed onto a magnet when the paper device was positioned in the magnetic holder. Apart from MB retention, this section also provided a lecture zone for the colorimetric readout. Finally, the third section was a circular end. This was allocated below an absorbent pad (26  $\times$  16 mm), which was produced using a guillotine and CF5. This pad functioned as a flow-driving absorbent pump and a waste storage unit.

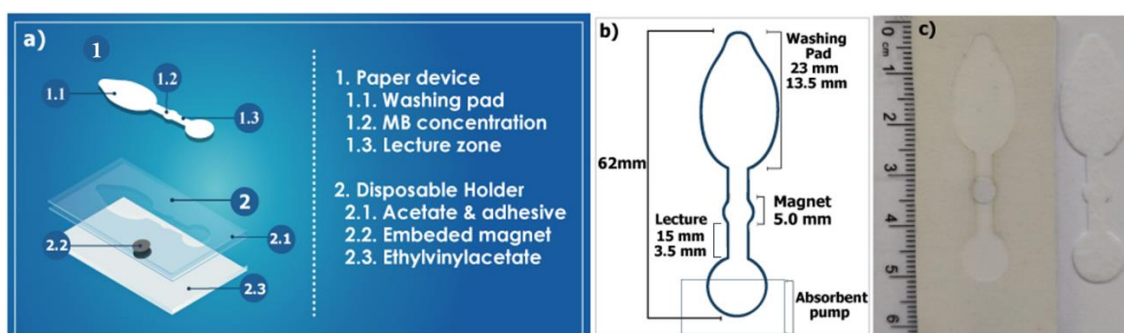


**Figure 1.** (a) Schematic representation of the system developed, which resembled that described in [28] but displayed different geometric features. (b) Dimensions of the single-piece paper device. (c) Picture of the reusable magnetic holder (left) and the disposable paper device produced with Standard 17 membrane (right).

On the other hand, the magnetic holder was a reusable device made of a first layer of ethylene-vinyl acetate (purchased from a local retailer). It displayed a pit that was made with a biopsy punch and accommodated a neodymium magnet (1 mm thick, 5 mm diameter). Two layers of acetate, carved with the Silhouette, were secured on top with double-sided adhesive. The bottom one was plain to keep the magnet in place and prevent direct contact with the MBs. The other displayed a cavity to accommodate the paper device and guarantee the correct alignment with the magnet. Once placed in the holder, the paper device fit in this cavity and sat directly onto the first acetate.

Paper devices were blocked by immersion in BSA 5%, Tween 0.5% for 15 min at room temperature, and were then washed twice with PBS-T for 3 min each. Finally, the devices were rinsed with water, dried for 30 min at 37.5 °C and stored in a ziplock pouch until used.

### 2.3. Smartphone Imaging System

A smartphone-integrated imaging system was designed to take photographs of the  $\mu$ PAD colorimetric readout (Figure S1 in Supplementary Material). This included a homemade dark box produced using a cardboard box (28 × 16 × 10 cm), a dimmable strip of white 6000K LED lights with a power of 1200 lm for lighting the chamber, and a smartphone placed on the lid, which had a hole for the phone camera. For image acquisition, paper devices were removed from the magnetic holders and were placed in the centre of the dark box. The box was closed, the lights were turned on, and images were obtained using the smartphone camera. When processing the images with ImageJ software, the signal at the detection pad was calculated for each paper device by subtracting the background registered for the whole device, converting the image into an 8-bit format and setting the colour threshold to 235 to obtain the mean grey value. Thus, the colorimetric signal was taken using the whole sensor area.

### 2.4. Pf-LDH Magneto-Immunodetection

Unless otherwise stated, MB modified with c-MAb (c-MAb-MB; Supporting information) were incubated in 1.5 mL Eppendorf tubes at 24 °C, protected from light in a thermoshaker (Thermal Shake lite, VWR International, Leuven, Belgium), and washed using a magnetic separator (BILATEST, Merck Life Science, Madrid, Spain).

#### 2.4.1. Magneto-Immunoassay in Tubes (Classical Approach)

The magneto-immunoassay originated from a previous development (Figure S2) [27,28]. Briefly, c-MAb-MB were washed two times with PBS and resuspended in PBST-BSA to a final concentration of 5 mg mL<sup>-1</sup>. Pf-LDH was then agitated at 1500 rpm for 5 min with 4  $\mu$ L of c-MAb-MB in PBST-BSA supplemented with bd-MAb (75 ng mL<sup>-1</sup>) and Poly-HRP (50 ng mL<sup>-1</sup>) in a final volume of 110  $\mu$ L. For spectrophotometric assay detection, the c-MAb-MB/Pf-LDH/bd-MAb/Poly-HRP complexes were washed twice with 150  $\mu$ L of PBST, resuspended in 100  $\mu$ L of

TMB and stirred for 20 min at 1500 rpm. After this, MBs were concentrated, the supernatant was transferred to 96-well plates, and 50  $\mu$ L of 1 M sulphuric acid was added to stop the reaction. Finally, absorbance was measured at 450 nm using a Sunrise plate reader (Tecan Group, Männedorf, Switzerland).

#### 2.4.2. Magneto-Immunoassay Using the $\mu$ PAD (POC Approach)

For on-chip MB washing and colorimetric assay detection, after the 5-min immunocapture performed in tubes (as indicated in Section 2.4.1), the mixture of c-MAb-MB/Pf-LDH/bd-MAb/Poly-HRP was directly placed in the  $\mu$ PAD washing pad. Four consecutive washes were next carried out by adding 100  $\mu$ L of PBST each time on the washing pad. Then, 50  $\mu$ L of TMB was added to the detection pad, where the magnetic complexes had been retained by a magnet, and the device was incubated for 5 min without agitation at room temperature before image capture.

#### 2.4.3. Pf-LDH Detection in Whole Blood Clinical Samples

Malaria patients and healthy individuals were recruited during the period of 2018–2020 at Vall d’Hebron University Hospital. Peripheral blood samples were obtained in heparin collection tubes before the administration of any antimalarial drugs. Malaria acute infections were confirmed by microscopy and/or PCR. The study was approved by the Ethics Committee of Vall d’Hebron University Hospital (PR(AG)30/2018), and the corresponding informed consent was obtained from all patients.

For detection of Pf-LDH using the  $\mu$ PAD, samples were diluted 1:1 with lysis buffer (50 mM  $\text{KH}_2\text{PO}_4$ , 300 mM NaCl, 0.25 M imidazole, 1% Triton X-100) and were incubated for 5 min at room temperature. Samples were diluted 1:10–1:100 with PBST-BSA and were processed as described in Section 2.4.2. All samples were analysed 2 times independently and were assayed in parallel by commercial RDT, microscopy and ELISA [29].

#### 2.5. Data Analysis

Paper devices were used just once (i.e., each device for a single Pf-LDH concentration). Except for the detection of clinical samples ( $n = 2$ ), graphs show the average of the colorimetric signal readout registered for no less than three independent replicates. In the same way, error bars correspond to the standard deviation (SD) of those replicates. The limit of detection (LOD) and the limit of quantification (LOQ) were calculated as the average of the signals registered for the blanks (i.e., experiments carried with all the reagents in the absence of Pf-LDH) plus 3 times and 10 times their SD, respectively. The sensitivity was calculated from the slope of the linear assay range. The variability was analysed in terms of coefficient of variation (% CV =  $(\text{SD}/\text{mean}) \times 100$ ). Signal-to-noise ratio (S/N) stands for the signal generated by each Pf-LDH concentration divided by the average signal registered for the blanks.

### 3. Results and Discussion

The starting point for this work was a single-step magneto-immunoassay developed previously for Pf-LDH detection [27], with some improvement (Figures 2a and S2) [28]. This consisted of a single 5-min incubation of the sample (lysed whole blood) with a cocktail of three reagents in an Eppendorf tube: cAb-MBs, which allowed fast Pf-LDH capture and concentration from whole blood; bd-MAb to grant binding specificity in a sandwich assay format; and Poly-HRP, an enzymatic signal amplifier formed by streptavidin and hundreds of HRP molecules that provided large signals. In the classical approach, this incubation was followed by two consecutive washing steps with PBS-T. Each washing step entailed placing the tube for 2 min in a magnetic rack for MB concentration, removing the supernatant without disturbing the MB pellet, and resuspending the MBs in the appropriate solution using a pipette. After the last wash, MBs were resuspended in TMB substrate solution, the Poly-HRP enzymatic reaction was allowed to proceed for 20 min, the tube was placed once more in the magnet for 2 min, and the supernatant was transferred to a 96-well plate

to quantitate colour intensity. Although fast and efficient in the hands of an expert, this procedure required user training and was incompatible with POC testing carried out by untrained personnel.

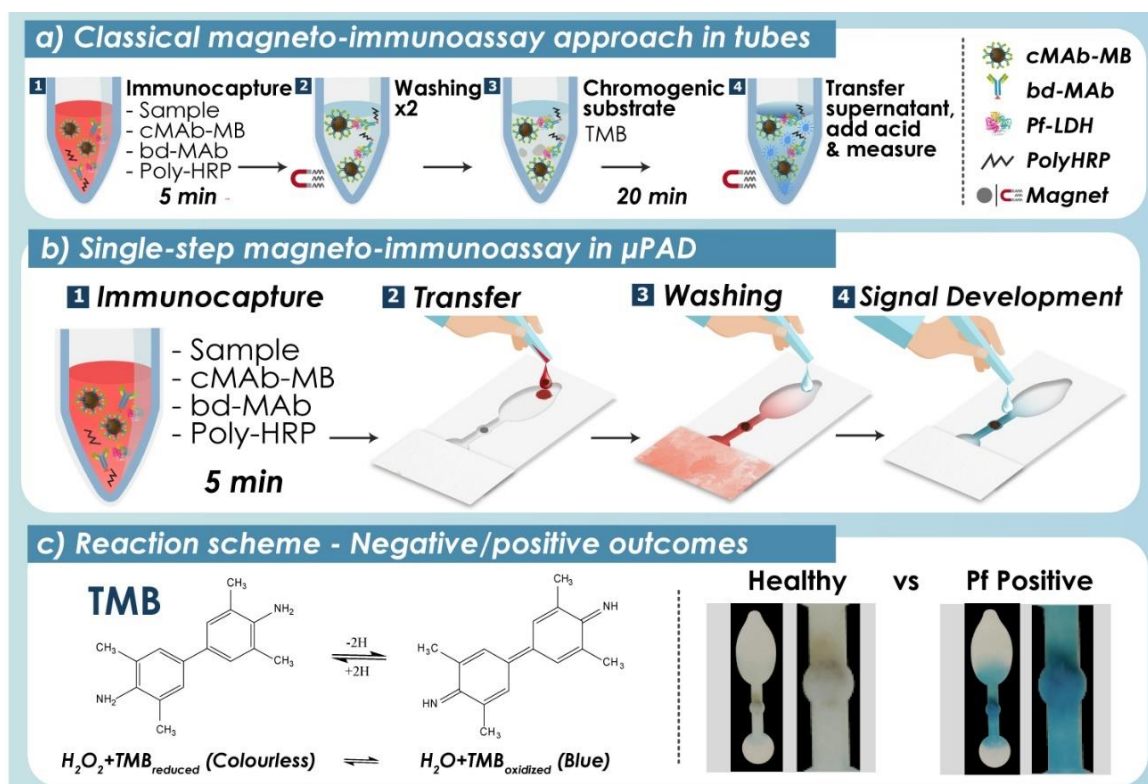


**Figure 2.** Single-step magneto-immunoassay carried out manually as reported in [28] (a) and using the  $\mu$ PAD developed here, which differed in size and shape from that in our previous work to better fit the requirements of colorimetric detection (b). (c) Scheme of TMB redox reaction (here, Poly-HRP catalyses TMB oxidation coupled to  $\text{H}_2\text{O}_2$  reduction for colour generation), and examples of negative and positive  $\mu$ PAD readouts.

The objective of this work was to demonstrate that this type of assay can be partially automated using a simple and inexpensive disposable  $\mu$ PAD (Figure 2b). Here, the colorimetric readout obtained has been interpreted alternatively by semi-quantitative visual inspection or using a smartphone camera and ImageJ free software, which provided quantitative results. Furthermore, this strategy entails the production of a universal paper device, which could be stored and employed to detect alternatively different magneto-immunoassays. The next sections summarize the optimization of the  $\mu$ PAD geometric features, magneto-immunoassay handling using the  $\mu$ PAD, and technology validation with clinical samples.

### 3.1. Production of the $\mu$ PAD

A  $\mu$ PAD was designed to carry out MB washing on-chip and under flow conditions. This device displayed three sections: a washing pad for the serial addition of the mixture of sample and reagents (c-MAB-MB, poly-HRP and bd-MAB) and the washing buffer; a pad for MB magnetic concentration and colour readout; and the final end with a staked absorbent pad (Figure 1). For its utilization, the  $\mu$ PAD was placed onto a reusable magnetic holder, which consisted of a piece of ethylene-vinyl acetate with an embedded magnet and a plastic cover that facilitated the alignment of the paper device.

The  $\mu$ PAD initially displayed a rectangular washing pad with smooth edges in order to facilitate solution flow and limit non-specific biocomponent retention. Figure 3a,b show 4 devices with washing pads of increasing area after adding the MBs in 100  $\mu\text{L}$  of a

stained solution, equivalent to the volume of sample and reagents used in the magneto-immunoassay. The two smallest washing pads tested (A1–A2) had a theoretical absorption capacity of 30 and 60  $\mu\text{L}$  and were able to absorb 100  $\mu\text{L}$  of solution only if these were pipetted very slowly, which was not practical. On the other hand, faster pipetting produced solution overflow, with the corresponding loss of MBs. The absorption pad in the A3 device absorbed this volume of solution in about 15 s, soaking the absorption and detection pads completely. In contrast, the largest absorption pad (A4), which had a theoretical adsorption capacity of 125  $\mu\text{L}$ , was not completely wet with this volume of solution, which increased the amount of washing buffer needed later on.

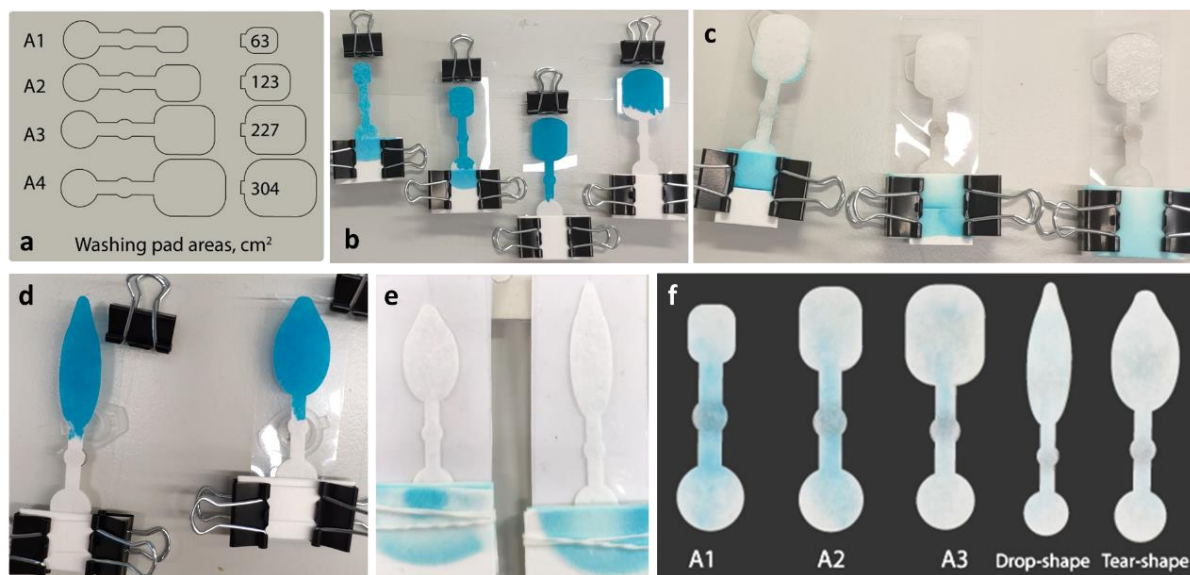


**Figure 3.** Production of the microfluidic paper device. (a) Design of paper devices with washing pads of increasing areas (A1–A4) and (b) their absorption capacity after adding MBs in 100  $\mu\text{L}$  of a stained solution. (c) Device A3, in which the 100  $\mu\text{L}$  of MB stained solution has been washed away after four consecutive additions of washing buffer of, from left to right, 50, 100, and 200  $\mu\text{L}$  each, while the MBs are retained magnetically in the detection zone (Figure S3). (d,e) Tear-shaped and drop-shaped devices before (d) and after (e) the stained solution has been washed away (4 washes, 100  $\mu\text{L}$  each). (f) Background noise obtained for the magneto-immunoassay, carried in 100  $\mu\text{L}$  of lysed whole blood (diluted 1:100) after washing 4 times (100  $\mu\text{L}$  each) and adding TMB substrate solution. Pictures of drop- and tear-shaped devices are not to scale.

In A3, 3–4 serial additions of 100  $\mu\text{L}$  of washing buffer were enough to wash the 100  $\mu\text{L}$  of stained solution and concentrate the MB in the retention zone (Figures 3c and S3). Lower washing volumes required more additions to accomplish washing and recover the MBs in the detection area, and larger volumes extended the washing steps unnecessarily. In all cases, the peripheral zones of the washing pad were washed less efficiently than the centre (Figure S3). This was concerning because the assay had to be carried out in lysed whole blood, and any unwashed cell debris and reagents could increase the background noise. Accordingly, the washing pad was re-designed to be either drop- or tear-shaped (Figure 3d,e). These two new designs had washing pad areas of around 250  $\text{cm}^2$  with elongated shapes and very smooth edges to minimise MB dispersion. These geometries granted fast adsorption of the 100  $\mu\text{L}$  of stained solution (Figure 3d), improved the flow of the MBs towards the magnet, and were washed efficiently (Figure 3e).

Finally, the best-performing designs (A1–A3, drop-shaped and tear-shaped) were used to determine MB on-chip washing efficiency. For this, lysed whole blood (Pf-LDH negative) was diluted at 1:100 in PBST-BSA and was incubated with c-MAb-MBs, bd-MAb and Poly-HRP for 5 min, and the mixture was transferred to the device washing pad. Four washes were carried out (100  $\mu\text{L}$  each), the adsorption pads were removed, and TMB was

added to the detection area (Figure 3f). Blue colour, attributed to poor washing, formed mainly in the vicinity of the lecture zone, with a significant decrease in colour intensity and dispersion as the washing pad area increased. The lowest background noise was observed for the drop and tear-shaped designs. This indicated that these washing pads provided the best MB washing and removal of leftover components.

### 3.2. Magneto-Immunoassay Handling and Detection Using the $\mu$ PAD

The operation of the magneto-immunoassay using the  $\mu$ PAD is illustrated in Figure 2b. The assay started with a single 5-min incubation of the sample/Pf-LDH and reagents (c-MAb-MB, poly-HRP and bd-MAb), which was carried out in a tube. The mixture was then transferred to the washing pad of the paper device. Washing buffer was added, which pushed the sample and reagents across the retention zone, where the MBs (and thus cMAb-MB/Pf-LDH/bd-MAb/Poly-HRP complexes in positive samples) were trapped magnetically. This stage was crucial because the washing buffer had to eliminate unbound reagents and non-targeted blood components, directing them towards the absorption pad in order to minimize background noise. Finally, 50  $\mu$ L of TMB enzyme substrate solution was added to the detection zone, and the device was incubated for 5 min in the dark for colour development. The formation of a blue product was indicative of the presence of Pf-LDH, and the colour intensity was proportional to the concentration of Pf-LDH.

The optimization of magneto-immunoassay performance under flow conditions included the study of the amount and location of TMB addition (Figure S4) and the concentration and type of c-MAb-MBs (Figures S5 and S6).

Dispensing the TMB in the centre of the detection zone directly onto the MBs produced MB random rearrangement, which reduced signal generation and reproducibility (Figure S4a). The highest colour intensity and reproducibility were achieved if the substrate solution was dispensed upstream from the magnet location in the stem that separated the washing and detection areas. Colour intensity also increased with the amount of TMB dispensed (30, 50 and 100  $\mu$ L), but both in the positive and the negative controls (background noise; Figure S4b). Therefore, the best S/N was achieved using 50  $\mu$ L of TMB (Figure S4). The amount of MBs used per sample was next decreased in an attempt to reduce the background noise, but the signals and S/N registered in the presence of Pf-LDH decreased as well, as did the assay sensitivity (slope) (Figure S5). A concentration of 20  $\mu$ g of c-MAb-MB per sample was selected for subsequent experiments. Invitrogen Dynabeads were tentatively substituted by GE SeraMag MB, which, according to the provider, display higher magnetic content. Although these exhibited faster magnetic concentration, they also provided slightly higher background noise and lower signals for all the concentrations of Pf-LDH studied. Accordingly, work continued with Dynabeads, which displayed higher signals for the Pf-LDH positive controls, lower background noise, and higher S/N in the magneto-immunoassay (Figure S6).

### 3.3. Quantitative Detection of Pf-LDH Using a Smartphone Detection System

Upon optimization, the paper-based magneto-immunoassay took less than 13 min, including single-step immunocapture, washing and detection. Colour intensity was proportional to Pf-LDH concentration between 3.13 ng mL<sup>-1</sup> and 100 ng mL<sup>-1</sup>, with an LOD of 6 ng mL<sup>-1</sup> (Figures 4a and S7), demonstrating the feasibility of carrying a semi-quantitative naked eye evaluation. The following step was implementing objective data acquisition and analysis using a smartphone.

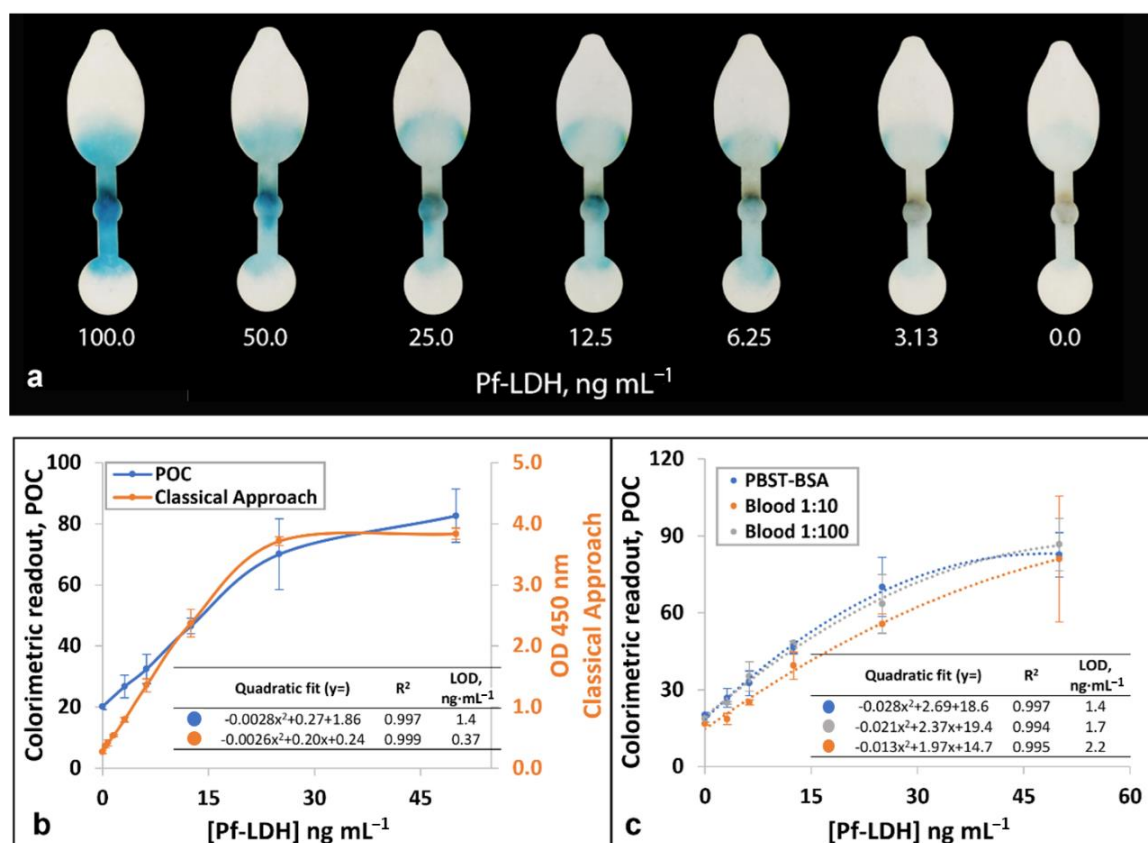


**Figure 4.** Signals registered in the paper-based magneto-immunoassay for different concentrations of Pf-LDH. (a) Photographs of the  $\mu$ PADs and results of semi-quantitative interpretation (Pf-LDH in PBST-BSA). (b) Signals obtained for the magneto-immunoassay carried in tubes using an ELISA reader (classical approach) and the  $\mu$ PAD using a smartphone and ImageJ ( $n = 4$ ; Figure S7). (c) Signals registered in the  $\mu$ PAD for Pf-LDH spiked in PBST-BSA or lysed blood (1:10 and 1:100 in PBST-BSA).

Smartphone-based densitometry can be challenging for POC applications due to the difficulty of controlling the positioning of the camera and compensating for the variable background noise. Accordingly, controlling a number of parameters, such as distance and angle between the camera and the paper device, light intensity, and area measured, is key to producing reproducible images and data. Here, an inexpensive dark box was produced for image acquisition using a cardboard box ( $28 \times 16 \times 10$  cm), modified with a strip of LEDs, used for lighting the chamber and controlling light exposure (Figure S1). A hole ( $2 \times 2$  cm) in the lid facilitated the correct positioning of any smartphone camera. Finally, pictures were processed using ImageJ, an open-source image analysis software that allowed subtracting the background noise before calculating colour intensity.

Image analysis of the results obtained in the  $\mu$ PAD for increasing concentrations of Pf-LDH (in PBST-BSA; Figures 4a and S7) allowed producing a calibration plot (Figure 4b). Compared to the assay in tubes, the smartphone-based  $\mu$ PAD produced higher background noise, attributed to less efficient MB washing, which resulted in higher LOD ( $0.37 \text{ ng mL}^{-1}$  in the assay in tubes;  $1.4 \text{ ng mL}^{-1}$  in the  $\mu$ PAD). Signal saturation was attained at a higher Pf-LDH concentration (50 instead of  $25 \text{ ng mL}^{-1}$ ), with variability between independent replicates below 18% (compared to  $<10\%$  in the classical approach).

A similar experiment was performed on spiked blood. For this, whole lysed blood from healthy individuals was diluted at 1:10 and 1:100 with PBST-BSA and spiked with  $0\text{--}100 \text{ ng}\cdot\text{mL}^{-1}$  of Pf-LDH. Finally, it was analysed using the smartphone-based  $\mu$ PAD. As shown in Figure S7, blood was washed away efficiently, and the devices did not display reddish blood leftovers. Furthermore, the calibration plots obtained in PBST-BSA and spiked blood (diluted 1:10 and 1:100) displayed comparable trends, with a linear response

between  $3.15 \text{ ng mL}^{-1}$  and  $25 \text{ ng mL}^{-1}$  of Pf-LDH concentration ( $R^2 > 0.99$ ) and signal saturation around  $50 \text{ ng mL}^{-1}$  (Figure 4c). In addition, the LODs were, in all cases, below  $2.2 \text{ ng mL}^{-1}$  of Pf-LDH. Considering that 1 parasite  $\mu\text{L}^{-1}$  corresponds to approximately  $0.2 \text{ ng mL}^{-1}$  of Pf-LDH [29], the LOD was under 11 parasites  $\mu\text{L}^{-1}$ . This was equivalent to 110 parasites  $\mu\text{L}^{-1}$  in prediluted samples when testing blood at 1:10, which is below the threshold value of 200 parasites  $\mu\text{L}^{-1}$  recommended by WHO for RDTs [13].

### 3.4. Analysis of Clinical Samples

The  $\mu\text{PAD}$  was finally employed to study a battery of whole blood samples (diluted 1:10 and 1:100), 9 from patients infected with *P. falciparum* and 8 from individuals either healthy or displaying infections unrelated to malaria (Figures 5a and S8). Samples were studied in parallel by standard microscopy and/or PCR at Vall d’Hebron Hospital and were also analysed by ELISA and one of the commercial RDT accredited by the WHO (Figure S9, Tables S1 and S2).

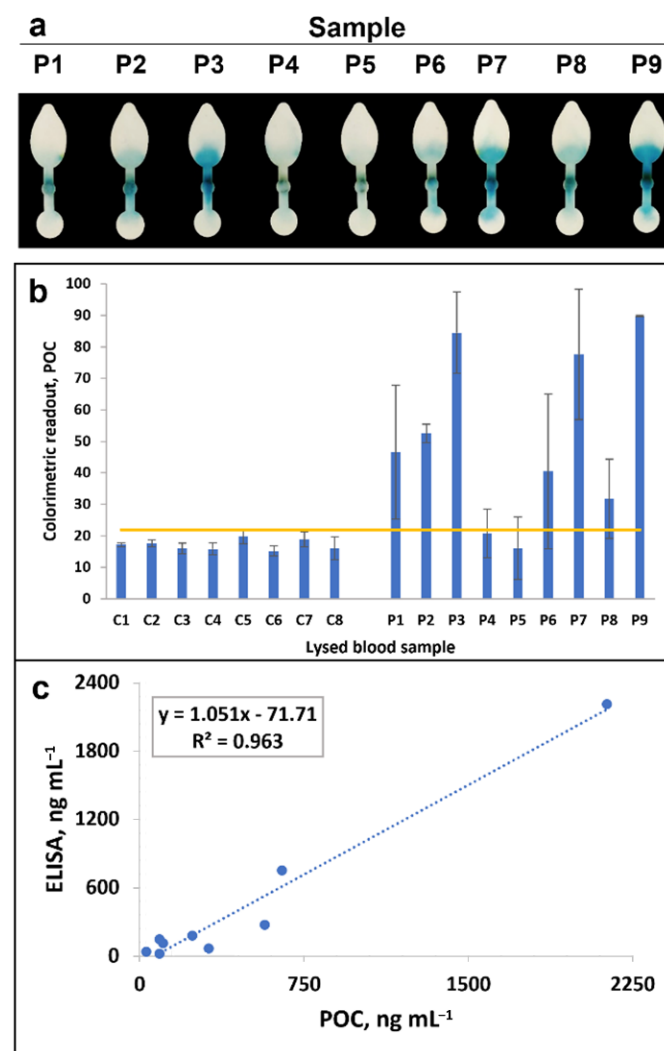


**Figure 5.** Detection of clinical whole blood samples using the  $\mu\text{PAD}$ . (a) Images of the colour readouts obtained in the  $\mu\text{PAD}$  for 9 blood samples obtained from patients infected with *P. falciparum* (lysed and diluted 1:10 with PBST-BSA). (b) Colorimetric readout obtained in samples negative (C1–8) or positive (P1–9) for *P. falciparum* (the horizontal line in the graph represents the analytical LOD, calculated from the signals and SD registered for the negative clinical samples). (c) Correlation of the concentration of Pf-LDH detected by the smartphone-based  $\mu\text{PAD}$  and the reference ELISA (samples diluted 1:10, except for sample P7, which was diluted to 1:100 due to signal saturation in the 1:10 dilution).

All the negative control samples displayed colour readouts that were below the POC LOD (Figure 5b). In contrast, 7 of the 9 malaria samples were clearly positive, exhibiting colour readouts above the test LOD, while the remaining two, which corresponded to submicroscopic malarias (negative by microscopy and confirmed by PCR and ELISA), displayed faint positives or negatives depending on the replicate. In positive samples, colour intensity visual interpretation allowed semi-quantitative result determination, with result agreement of 80–91% among untrained individuals (Figure S10). Furthermore, the concentration of Pf-LDH detected using the smartphone-based  $\mu$ PAD correlated with that obtained by ELISA (Figure 5c), providing quantitative results faster and with less handling.

Lastly, the samples were analysed using a commercial RDT, which detected in parallel Pf-HRP2 and pLDH. Although most commercial RDTs afford LODs in the range of 0.4–1.6 ng mL<sup>-1</sup> when detecting Pf-HRP2, the few tests that detect pLDH display LODs spanning 10–1000 ng mL<sup>-1</sup> [30]. This difference has also been noticed by several authors. For example, the multiplexed ELISA reported by Jang et al. exploited Quansys Q-Plex technology and exhibited LODs of 2.3, 47.8, and 75.1 pg mL<sup>-1</sup> for HRP2, pLDH and *P. vivax* LDH (Pv-LDH), respectively [31]. The Luminex fluorescent assay developed by Marti nez-Vendrell and co-workers detected HRP2, Pf-LDH and Pv-LDH with LODs of 6, 56 and 1093 pg mL<sup>-1</sup> [32], respectively. Additionally, the multiplexed  $\mu$ PAD produced by Deraney and co-workers detected Pf-HRP2 and pLDH with LODs of 20.3 ng mL<sup>-1</sup> and 80.2 ng mL<sup>-1</sup>, respectively [25]. Here, of the 9 malaria samples tested with the RDT, only 2 provided faintly positive test lines for pLDH, while the HRP2 result was positive in 7 and negative (P5) or faintly positive (P1) in the other 2 (Figure S9).

In summary, the  $\mu$ PAD developed here achieved remarkable results when tested against a commercial RDT, detecting malaria samples better than the RDT pLDH test and similarly to the Pf-HRP2 test. Furthermore, the device provided quantitative readouts that correlated with those obtained using standard methods (Table S1). Despite the small number of samples studied, these results show that the technology developed provides fast quantitative results, entailing little user intervention and a cost per test below 0.5   (Table S3).

#### 4. Conclusions

A  $\mu$ PAD has been developed that provides the smooth operation of single-step magneto-immunoassays, including MB magnetic concentration, washing and incubation with a chromogenic enzyme substrate. As has been shown, visual inspection of the colorimetric readout provides a semi-quantitative interpretation, while image capture and analysis using a smartphone camera and ImageJ deliver analyte quantification.

As a proof-of-concept, the system has been employed to detect Pf-LDH, a biomarker of malaria infection. Malaria antibody-based RDTs display turnaround times of 15–30 min and prices in the range of (1–5  ), delivering qualitative results. The  $\mu$ PAD developed in this work afforded quantitative Pf-LDH detection in lysed blood diluted 1:10 in <20 min (including 5 min of sample lysis), with LODs of 6.25 ng·mL<sup>-1</sup> and 1.4 ng·mL<sup>-1</sup> when interpreted by the naked eye and imaging analysis, respectively. Considering 1 parasite  $\mu$ L<sup>-1</sup> equivalent to 0.06–0.2 ng·mL<sup>-1</sup>, these LODs correspond to 7–23 and 31–104 parasites  $\mu$ L<sup>-1</sup>, which is below the cut-off of 200 parasites  $\mu$ L<sup>-1</sup> recommended by the WHO for RDTs. Furthermore, Pf-LDH quantitation provided by the  $\mu$ PAD correlated with that granted by the reference ELISA, but the  $\mu$ PAD was faster and easier to use.

Using the paper device to automate a magneto-immunoassay, rather than incorporating the biocomponents on-chip, converts the system into a versatile universal platform, easier to tune than classical RDTs by just changing the analyte in the single-step magneto-immunoassay step. With a low estimated production cost and result interpretation using a common smartphone, this  $\mu$ PAD is a versatile platform that could facilitate cost-effective POC testing in remote and low-resource settings.

**Supplementary Materials:** The following supporting information can be downloaded at: <https://www.mdpi.com/article/10.3390/bios12090680/s1>, Figure S1: Optimization home-made light controlled box; Figure S2: Comparison of the single-step magneto-immunoassay developed in this work versus the assay previously developed; Figure S3: Geometrical evolution, washing strategy and signal intensity in the negative controls; Figure S4: Optimization of dispensing position and amount of TMB used in the  $\mu$ PAD for magneto-immunoassay detection; Figure S5: Optimization of the concentration of MBs in the paper-based magneto-immunoassay; Figure S6: Comparative performance of MBs from Invitrogen and GE Healthcare; Figure S7: Detection of Pf-LDH in PBST-BSA and blood using the POC device; Figure S8: Study of clinical samples using the POC device; Figure S9: Study of clinical samples using a commercial RDT; Figure S10: External evaluation of semiquantitative naked eye colour scale; Table S1: Summary of the results obtained in the analysis of clinical samples from malaria patients; Table S2: Summary of the results obtained for the control blood samples; Table S3: Estimate of the production cost of the retail-purchased reagents of  $\mu$ PAD.

**Author Contributions:** Conceptualization, K.A.-A. and E.B.; methodology and investigation, K.A.-A., A.S.-C. and J.P.-T.; validation, K.A.-A., P.B.-N., E.S. and I.O.; data curation, E.S. and A.S.-M.; writing—original draft preparation, K.A.-A.; writing—review and editing, A.S.-M. and E.B.; supervision, E.B.; funding acquisition, I.M. and E.B. All authors have read and agreed to the published version of the manuscript.

**Funding:** This research was funded by Fondo de Investigaciones Sanitarias of Instituto de Salud Carlos III (co-funded by the European Regional Development Fund; grants CPII18/00025, IFI18/00020, JR18/00022 and QUPID EuroNanoMed AC21\_2/00021) and La Caixa Foundation (ID 100010434, fellowship LCF/BQ/DI18/11660061). Diagnostic Nanotools is a consolidated group supported by Secretaria d'Universitats i Recerca, Generalitat de Catalunya (2017 SGR 240).

**Institutional Review Board Statement:** This study was conducted in accordance with the Declaration of Helsinki, and approved by the Ethics Committee of Vall d'Hebron University Hospital (PR(AG)30/2018).

**Informed Consent Statement:** Informed consent was obtained from all subjects involved in this study.

**Acknowledgments:** The authors thank the 483 volunteers who kindly answered the 3 questioners shown in Figure S10.

**Conflicts of Interest:** The authors declare no conflict of interest.

## References

1. Wang, C.M.; Chen, C.Y.; Liao, W.S. Enclosed Paper-Based Analytical Devices: Concept, Variety, and Outlook. *Anal. Chim. Acta* **2021**, *1144*, 158–174. [[CrossRef](#)] [[PubMed](#)]
2. Nishat, S.; Jafry, A.T.; Martinez, A.W.; Awan, F.R. Paper-Based Microfluidics: Simplified Fabrication and Assay Methods. *Sens. Actuators B Chem.* **2021**, *336*, 129681. [[CrossRef](#)]
3. Heidt, B.; Siqueira, W.F.; Eersels, K.; Diliën, H.; Van Grinsven, B.; Fujiwara, R.T.; Cleij, T.J. Point of Care Diagnostics in Resource-Limited Settings: A Review of the Present and Future of PoC in Its Most Needed Environment. *Biosensors* **2020**, *10*, 133. [[CrossRef](#)] [[PubMed](#)]
4. Nguyen, V.T.; Song, S.; Park, S.; Joo, C. Recent Advances in High-Sensitivity Detection Methods for Paper-Based Lateral-Flow Assay. *Biosens. Bioelectron.* **2020**, *152*, 112015. [[CrossRef](#)]
5. Shirshahi, V.; Liu, G. Enhancing the Analytical Performance of Paper Lateral Flow Assays: From Chemistry to Engineering. *Trends Anal. Chem.* **2021**, *136*, 116200. [[CrossRef](#)]
6. Cowman, A.F.; Healer, J.; Marapana, D.; Marsh, K. Malaria: Biology and Disease. *Cell* **2016**, *167*, 610–624. [[CrossRef](#)]
7. WHO. *World Malaria Report 2021*; World Health Organization: Geneva, Switzerland, 2021.
8. WHO. *Report on Antimalarial Drug Efficacy, Resistance and Response: 10 Years of Surveillance (2010–2019)*; World Health Organization: Geneva, Switzerland, 2020.
9. Monge-Maillou, B.; Jiménez, B.C.; Pérez-Molina, J.A.; Norman, F.; Navarro, M.; Pérez-Ayala, A.; Herrero, J.M.; Zamarrón, P.; López-Vélez, R. Imported Infectious Diseases in Mobile Populations, Spain. *Emerg. Infect. Dis.* **2009**, *15*, 1745–1752. [[CrossRef](#)]
10. Caminade, C.; Kovats, S.; Rocklöv, J.; Tompkins, A.M.; Morse, A.P.; Colón-González, F.J.; Stenlund, H.; Martens, P.; Lloyd, S.J. Impact of Climate Change on Global Malaria Distribution. *Proc. Natl. Acad. Sci. USA* **2014**, *111*, 3286–3291. [[CrossRef](#)]
11. Mouatcho, J.C.; Dean Goldring, J.P. Malaria Rapid Diagnostic Tests: Challenges and Prospects. *J. Med. Microbiol.* **2013**, *62*, 1491–1505. [[CrossRef](#)]

12. Wu, L.; Van Den Hoogen, L.L.; Slater, H.; Walker, P.G.T.; Ghani, A.C.; Drakeley, C.J.; Okell, L.C. Comparison of Diagnostics for the Detection of Asymptomatic Plasmodium Falciparum Infections to Inform Control and Elimination Strategies. *Nature* **2015**, *528*, S86–S93. [[CrossRef](#)]
13. WHO. *WHO Guidelines for Malaria*; World Health Organization: Geneva, Switzerland, 2021.
14. Mukkala, A.N.; Kwan, J.; Lau, R.; Harris, D.; Kain, D.; Boggild, A.K. An Update on Malaria Rapid Diagnostic Tests. *Curr. Infect. Dis. Rep.* **2018**, *20*, 49. [[CrossRef](#)] [[PubMed](#)]
15. Gendrot, M.; Fawaz, R.; Dormoi, J.; Madamet, M.; Pradines, B. Genetic Diversity and Deletion of Plasmodium Falciparum Histidine-Rich Protein 2 and 3: A Threat to Diagnosis of P. Falciparum Malaria. *Clin. Microbiol. Infect.* **2019**, *25*, 580–585. [[CrossRef](#)] [[PubMed](#)]
16. Yerlikaya, S.; Campillo, A.; Gonzalez, I.J. A Systematic Review: Performance of Rapid Diagnostic Tests for the Detection of Plasmodium Knowlesi, Plasmodium Malariae, and Plasmodium Ovale Monoinfections in Human Blood. *J. Infect. Dis.* **2018**, *218*, 265–276. [[CrossRef](#)] [[PubMed](#)]
17. Abrahamson, S.S. *The State of the Malaria RDT Market 2018*; World Health Organization: Geneva, Switzerland, 2018.
18. Kavanaugh, M.J.; Azzam, S.E.; Rockabrand, D.M. Malaria Rapid Diagnostic Tests: Literary Review and Recommendation for a Quality Assurance, Quality Control Algorithm. *Diagnostics* **2021**, *11*, 768. [[CrossRef](#)] [[PubMed](#)]
19. Rei Yan, S.L.; Wakasuqui, F.; Wrenger, C. Point-of-Care Tests for Malaria: Speeding up the Diagnostics at the Bedside and Challenges in Malaria Cases Detection. *Diagn. Microbiol. Infect. Dis.* **2020**, *98*, 115122. [[CrossRef](#)]
20. Dos Santos, G.P.; Corrêa, C.C.; Kubota, L.T. A Simple, Sensitive and Reduced Cost Paper-Based Device with Low Quantity of Chemicals for the Early Diagnosis of Plasmodium Falciparum Malaria Using an Enzyme-Based Colorimetric Assay. *Sens. Actuators B* **2018**, *255*, 2113–2120. [[CrossRef](#)]
21. Nolder, D.; Stewart, L.; Tucker, J.; Ibrahim, A.; Gray, A.; Corrah, T.; Gallagher, C.; John, L.; O'Brien, E.; Aggarwal, D.; et al. Failure of Rapid Diagnostic Tests in Plasmodium Falciparum Malaria Cases in UK Travellers: Identification and Characterisation of the Parasites. *Int. J. Infect. Dis.* **2021**, *108*, 137–144. [[CrossRef](#)]
22. WHO. *World Malaria Report 2019*; World Health Organization: Geneva, Switzerland, 2019.
23. Atchade, P.S.; Doderer-Lang, C.; Chabi, N.; Perrotey, S.; Abdelrahman, T.; Akpovi, C.D.; Anani, L.; Bigot, A.; Sanni, A.; Candolfi, E. Is a Plasmodium Lactate Dehydrogenase (PLDH) Enzyme-Linked Immunosorbent (ELISA)-Based Assay a Valid Tool for Detecting Risky Malaria Blood Donations in Africa? *Malar. J.* **2013**, *12*, 279. [[CrossRef](#)]
24. Nyataya, J.; Waitumbi, J.; Mobegi, V.A.; Noredin, A.; El Zowalaty, M.E. Plasmodium Falciparum Histidine-Rich Protein 2 and 3 Gene Deletions and Their Implications in Malaria Control. *Diseases* **2020**, *8*, 15. [[CrossRef](#)]
25. Deraney, R.N.; Mace, C.R.; Rolland, J.P.; Schonhorn, J.E. Multiplexed, Patterned-Paper Immunoassay for Detection of Malaria and Dengue Fever. *Anal. Chem.* **2016**, *88*, 6161–6165. [[CrossRef](#)]
26. Singh, N.K.; Jain, P.; Das, S.; Goswami, P. Dye Coupled Aptamer-Captured Enzyme Catalyzed Reaction for Detection of Pan Malaria and P. falciparum Species in Laboratory Settings and Instrument-Free Paper-Based Platform. *Anal. Chem.* **2019**, *91*, 4213–4221. [[CrossRef](#)] [[PubMed](#)]
27. Ruiz-Vega, G.; Arias-Alpizar, K.; de la Serna, E.; Borgheti-Cardoso, L.N.; Sulleiro, E.; Molina, I.; Fernández-Busquets, X.; Sánchez-Montalvá, A.; del Campo, F.J.; Baldrich, E. Electrochemical POC Device for Fast Malaria Quantitative Diagnosis in Whole Blood by Using Magnetic Beads, Poly-HRP and Microfluidic Paper Electrodes. *Biosens. Bioelectron.* **2020**, *150*, 111925. [[CrossRef](#)]
28. Arias-Alpizar, K.; Sánchez-Cano, A.; Prat-Trunas, J.; de la Serna, E.; Alonso, O.; Sulleiro, E.; Sánchez-Montalvá, A.; Diéguez, A.; Baldrich, E. Malaria quantitative POC testing using magnetic particles, a paper microfluidic device and a hand-held fluorescence reader. *Biosens. Bioelectron.* **2022**, *215*, 114513. [[CrossRef](#)]
29. De la Serna, E.; Arias-Alpizar, K.; Borgheti-Cardoso, L.N.; Sanchez-Cano, A.; Sulleiro, E.; Zarzuela, F.; Bosch-Nicolau, P.; Salvador, F.; Molina, I.; Ramírez, M.; et al. Detection of Plasmodium Falciparum Malaria in 1 h Using a Simplified Enzyme-Linked Immunosorbent Assay. *Anal. Chim. Acta* **2021**, *1152*, 338254. [[CrossRef](#)] [[PubMed](#)]
30. Jimenez, A.; Rees-Channer, R.R.; Perera, R.; Gamboa, D.; Chiodini, P.L.; González, I.J.; Mayor, A.; Ding, X.C. Analytical Sensitivity of Current Best-in-Class Malaria Rapid Diagnostic Tests. *Malar. J.* **2017**, *16*, 128. [[CrossRef](#)] [[PubMed](#)]
31. Jang, I.K.; Tyler, A.; Lyman, C.; Kahn, M.; Kalnoky, M.; Rek, J.C.; Arinaitwe, E.; Adrama, H.; Murphy, M.; Imwong, M.; et al. Simultaneous Quantification of Plasmodium Antigens and Host Factor C-Reactive Protein in Asymptomatic Individuals with Confirmed Malaria by Use of a Novel Multiplex Immunoassay. *J. Clin. Microbiol.* **2019**, *57*, e00948-18. [[CrossRef](#)]
32. Martiáñez-Vendrell, X.; Jiménez, A.; Vázquez, A.; Campillo, A.; Incardona, S.; González, R.; Gamboa, D.; Torres, K.; Oyibo, W.; Faye, B.; et al. Quantification of Malaria Antigens PfHRP2 and PLDH by Quantitative Suspension Array Technology in Whole Blood, Dried Blood Spot and Plasma. *Malar. J.* **2020**, *19*, 12. [[CrossRef](#)]

# **Magnetic bead handling using a paper-based device for quantitative point-of-care testing**

## ***Supplementary Material***

Kevin Arias-Alpízar <sup>1,2</sup>, Ana Sánchez-Cano <sup>1,2</sup>, Judit Prat-Trunas <sup>1</sup>, Elena Sulleiro <sup>2,3,4</sup>, Pau Bosch-Nicolau <sup>3,4</sup>, Fernando Salvador <sup>3,4</sup>, Inés Oliveira <sup>3,4</sup>, Israel Molina <sup>3,4</sup>, Adrián Sánchez-Montalvá <sup>2,3,4</sup> and Eva Baldrich <sup>1,4,\*</sup>

<sup>1</sup> *Diagnostic Nanotools Group, Vall d'Hebron Institut de Recerca (VHIR), 08035 Barcelona, Spain*

<sup>2</sup> *Universitat Autònoma de Barcelona (UAB), 08193 Bellaterra (Barcelona), Spain*

<sup>3</sup> *International Health Unit Vall d'Hebron-Drassanes, Vall d'Hebron Hospital Universitari, PROSICS  
Barcelona, 08035 Barcelona, Spain*

<sup>4</sup> *Centro de Investigación Biomédica en Red de Enfermedades Infecciosas (CIBERINFEC), Instituto de  
Salud Carlos III, 28028 Madrid, Spain*

\* Correspondence: [eva.baldrich@vhir.org](mailto:eva.baldrich@vhir.org)

## **Table of contents:**

### **Material and methods.**

Production of biotinylated detection antibodies (bd-Ab).

MB modification with c-MAb using EDC.

### **Results and discussion.**

**Figure S1.** Optimization home-made light controlled box.

**Figure S2.** Comparison of the single-step magneto-immunoassay developed in this work *versus* the assay previously developed.

**Figure S3.** Geometrical evolution, washing strategy and signal intensity in the negative controls.

**Figure S4.** Optimization of dispensing position and amount of TMB used in the  $\mu$ PAD for magneto-immunoassay detection.

**Figure S5.** Optimization of the concentration of MBs in the paper-based magneto-immunoassay.

**Figure S6.** Comparative performance of MBs from Invitrogen and GE Healthcare.

**Figure S7.** Detection of Pf-LDH in PBST-BSA and blood using the POC device.

**Figure S8.** Study of clinical samples using the POC device.

**Figure S9.** Study of clinical samples using a commercial RDT.

**Figure S10.** External evaluation of semiquantitative naked eye colour scale.

**Table S1.** Summary of the results obtained in the analysis of clinical samples from malaria patients.

**Table S2.** Summary of the results obtained for the control blood samples.

**Table S3.** Estimate of the production cost of the retail-purchased reagents of  $\mu$ PAD (indirect and personnel costs not included).

## Material and Methods

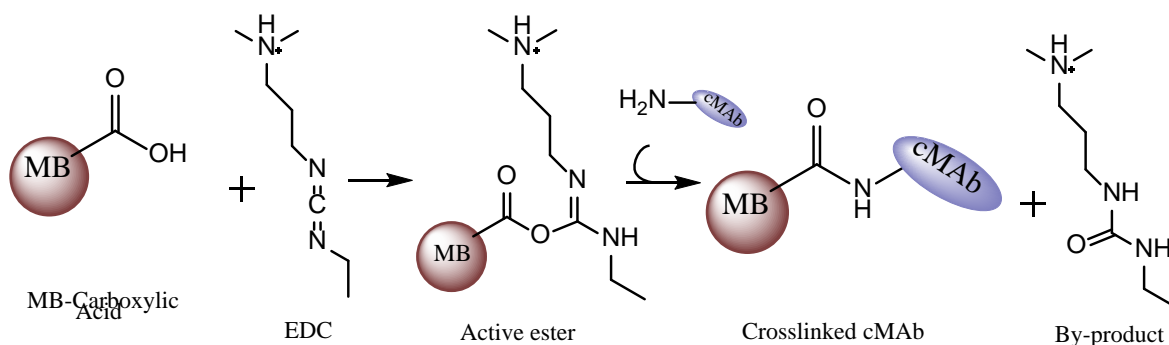
### Production of biotinylated detection antibodies (bd-MAb).

The detection antibody (d-MAb) was first submitted to a buffer interchange in order to remove interfering reagents. For this, 300 µg of d-MAb were placed in an Amicon® Ultra 0.5 mL Centrifugal Filter (Merck Life Science, Madrid, Spain) in a final volume of 0.5 mL. The device was centrifuged at 14000 x g for 10 min, was filled with 0.5 mL of sodium carbonate buffer (0.1 M, pH 9.5), and was centrifuged again. This procedure was repeated once more. The concentrated d-MAb was then recovered, and sodium carbonate buffer was added to bring it to the initial concentration of 4.1 mg·mL<sup>-1</sup>.

A biotin-XX, SSE (6-((6-((Biotinoyl)Amino)Hexanoyl)amino)Hexanoic Acid, Sulfosuccinimidyl Ester, Sodium Salt; Ref. B6352, Thermo Fisher Scientific; Barcelona, Spain) stock was prepared at a concentration of 2.5 mg·mL<sup>-1</sup> in Milli-Q water and 9.66 µL were added to the d-MAb. The mixture was stirred at 24°C in the dark for 2 h. The biotin not bound to the d-MAb was eliminated using a PD G25 exclusion column (GE Healthcare, now Cytiva Europe, Freiburg, Germany) following the provider's instructions. The obtained bd-MAb was finally diluted to a concentration of 150 µg·mL<sup>-1</sup> in 1% BSA and was stored at -20 °C.

### MB modification with c-MAb using EDC

MB (1 mg in 100 µL) were washed twice with 15 mM MES using a magnetic separator (BILATEST, Merk). MB were next agitated for 15 min with 25 µg of c-MAb in 100 µL of 2 mg·mL<sup>-1</sup> EDC in a thermoshaker (950 rpm; Thermal Shake lite; VWR International, Leuven, Belgium). After that, MB were serially washed with 200 µL of MES and PBS, and were blocked for 1 h with PBS, BSA 1%. The c-MAb-MB were then washed twice for 5 min with 100 µL of PBS, Tween 20 0.1% and were resuspended in 500 µL of PBS, Tween 20 0.1%, BSA 0.2% for storage at 4 °C (1.4-2.4×10<sup>9</sup> MB·mL<sup>-1</sup>, equivalent to 2 mg·mL<sup>-1</sup>). The following figure illustrates the chemical reaction involved.



## Figures

**Figure S1. Home-made dark box with controlled lighting.** (Left) A dark box was produced for image acquisition using a cardboard box (28cmx16cm x10cm), modified with a strip of LED lights (cool white 6000K LED dimmable strip lights with a power of 1200 lm) used for lighting the chamber. (Right) A smartphone was placed on top of the lid, which had a hole for the phone camera. The photograph shows the dark box placed upside-down.

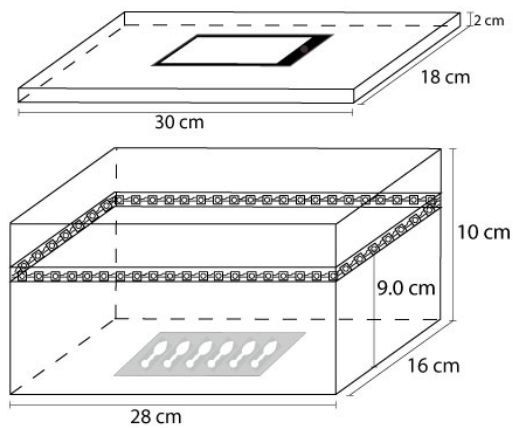


**Figure S2. Comparison of the single-step magneto-immunoassay developed in this work versus the assay previously developed.**

The starting point for this work was a single-step magneto-immunoassay developed previously for Pf-LDH detection, with some improvement [1,2]. That magneto-immunoassay relied on a customized nanoconjugate, produced by incubating bd-MAb and polyHRP (bd-MAb-polyHRP). A single-step magneto-immunoassay was next carried, which consisted in a single 5-min incubation of the sample (diluted with 1×RD to a final volume of 95 µL) with c-MAb-MB (4 µL) and the bd-MAb/Poly-HRP conjugate (0.5 µL; final concentration of bd-MAb and Poly-HRP of 225 ng mL<sup>-1</sup> and 50 ng mL<sup>-1</sup>, respectively). MB were then washed twice with 150 µL of PBST, and were stirred for 20 min in 100 µL of TMB substrate solution. After this, MBs were concentrated, the supernatant was transferred to 96-well plates, 50 µL of 1 M sulphuric acid were added to each well, and colorimetric detection was carried at 450 nm using a Sunrise plate reader (Tecan Group, Männedorf, Switzerland).

Although both bd-MAb and Poly-HRP were storage-stable, the bd-MAb/Poly-HRP conjugate was stable for a just month. In addition, the assay displayed a narrow linear range, with signal saturation above 12.5 ng mL<sup>-1</sup> of Pf-LDH.

To overcome these drawbacks, here we used an optimized magneto-immunoassay (Figure 2a in the main manuscript), in which samples were incubated for 5 min with a cocktail of three reagents: c-MAb-MB (4 µL), bd-MAb (75 ng mL<sup>-1</sup>) and Poly-HRP (50 ng mL<sup>-1</sup>). As it can be observed in the graphs, this new assay displays similar signals (a) and signal-to-noise ratios (S/N; b) than the previous one for low-to-mid Pf-LDH concentrations, but higher signals and S/N for Pf-LDH concentrations ranging 10-50 ng mL<sup>-1</sup> and wider linear range.

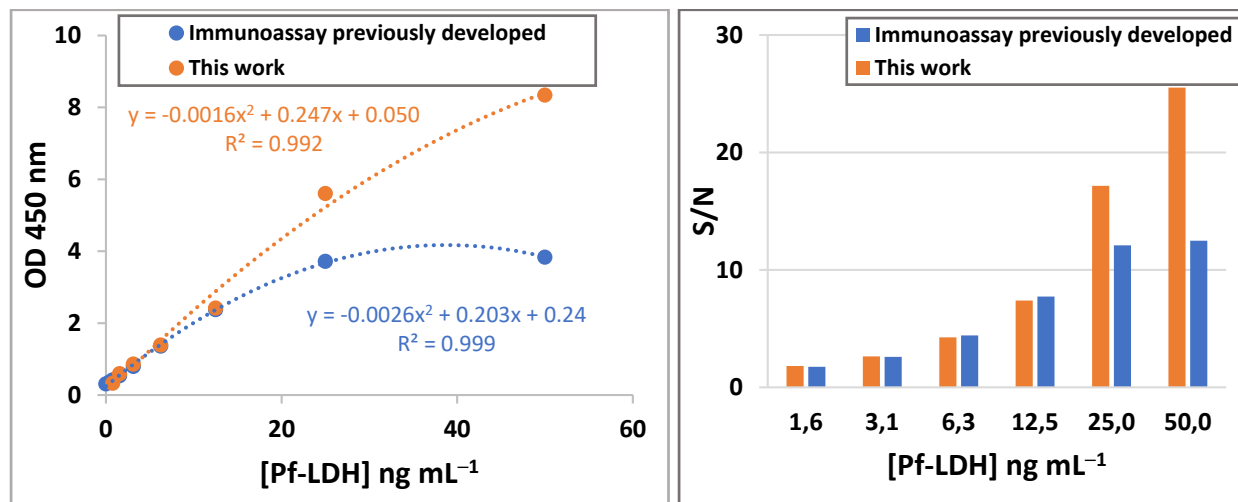


**Figure S3. Geometrical evolution, washing strategy and signal intensity in the negative controls.**

MB washing under flow conditions was optimized by mixing the MBs with 100  $\mu\text{L}$  of a blue-stained aqueous solution. The mixture was then pipetted onto the washing pad of the devices. These had been placed onto a piece of acetate with a magnet for MB retention at the detection area, and with a pile of absorbent pads at the bottom. Serial additions of PBS 0.1x were then made, using alternatively 50, 100 or 200  $\mu\text{L}$  of solution per wash. As it can be observed, for 50- $\mu\text{L}$  additions, 5 consecutive washes were needed to remove completely the stained solution and observe the MBs concentrated in the central retention zone. For 100-200  $\mu\text{L}$  washing volumes, 3-4 additions were enough. However, the addition 200  $\mu\text{L}$  per washing volume saturated the paper sensor (sensor volume capacity  $\approx 150$   $\mu\text{L}$ ), which caused solution overflow, less efficient dye washing, and loss of MBs. In all the cases, and independently of the washing conditions, MPs were retained efficiently by the magnet in the detection area which could be seen by the naked eye.

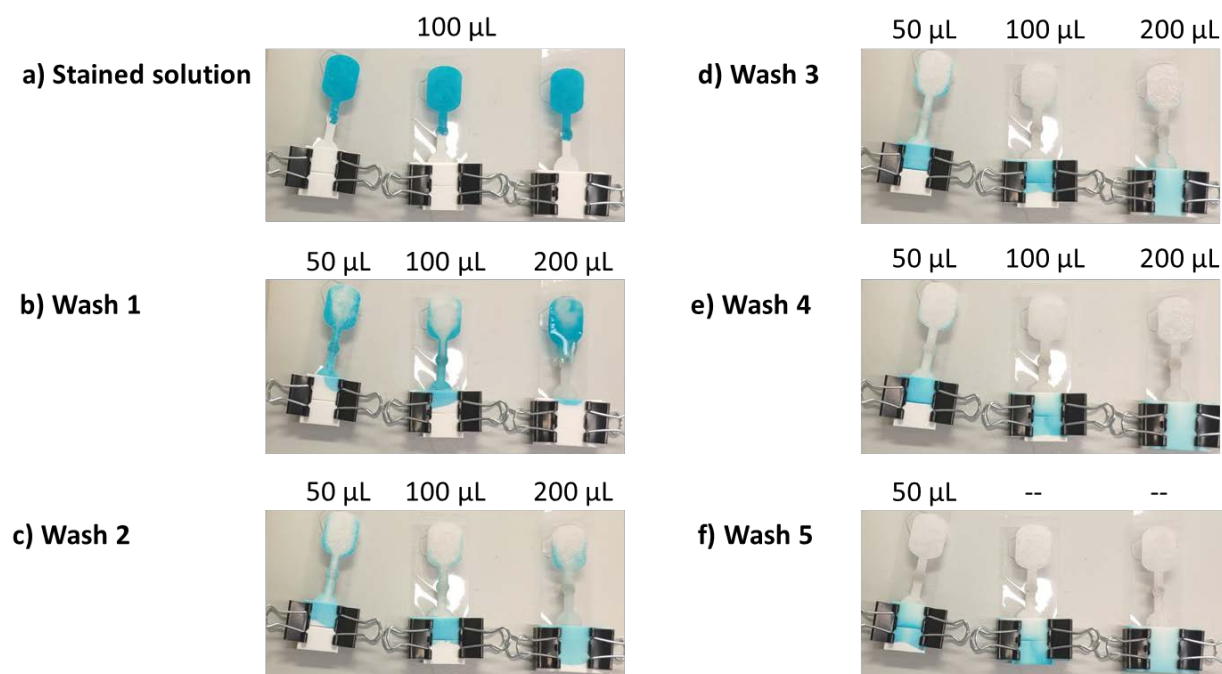


**Figure S4. Optimization of dispensing position and amount of TMB used in the  $\mu$ PAD for magneto-immunoassay detection.**

a) Examples of the colorimetric readouts obtained in the paper-based magneto-immunoassay for a positive control ( $25 \text{ ng}\cdot\text{mL}^{-1}$  of Pf-LDH) after dropping for detection  $50 \mu\text{L}$  of TMB in three different positions. Dispensing the TMB directly onto the MBs (position 3) produced MB random rearrangement, decreasing signal intensity and reproducibility. Higher colour intensity and signal reproducibility were achieved if the substrate solution was dispensed upstream (positions 1 and 2). However, placing TMB too far from the MBs (i.e., position 1) facilitated TMB reflow towards the washing zone. This decrease TMB availability and colour evolution at the detection zone. Position 2 was chosen because it produced a more homogenous colour dispersion around the magnet and lower background signal in the blanks. b) Colorimetric readouts obtained for positive and negative controls ( $25$  and  $0 \text{ ng}\cdot\text{mL}^{-1}$  of Pf-LDH, respectively) when using for detection increasing volumes of TMB (dropped at position 2). A slight increment in the signals (both positive and negative) was observed when using increasing volumes of TMB, which was attributed to longer reaction times before substrate exhaustion occurred. The best signal-to-noise was achieved using  $50 \mu\text{L}$  of TMB.

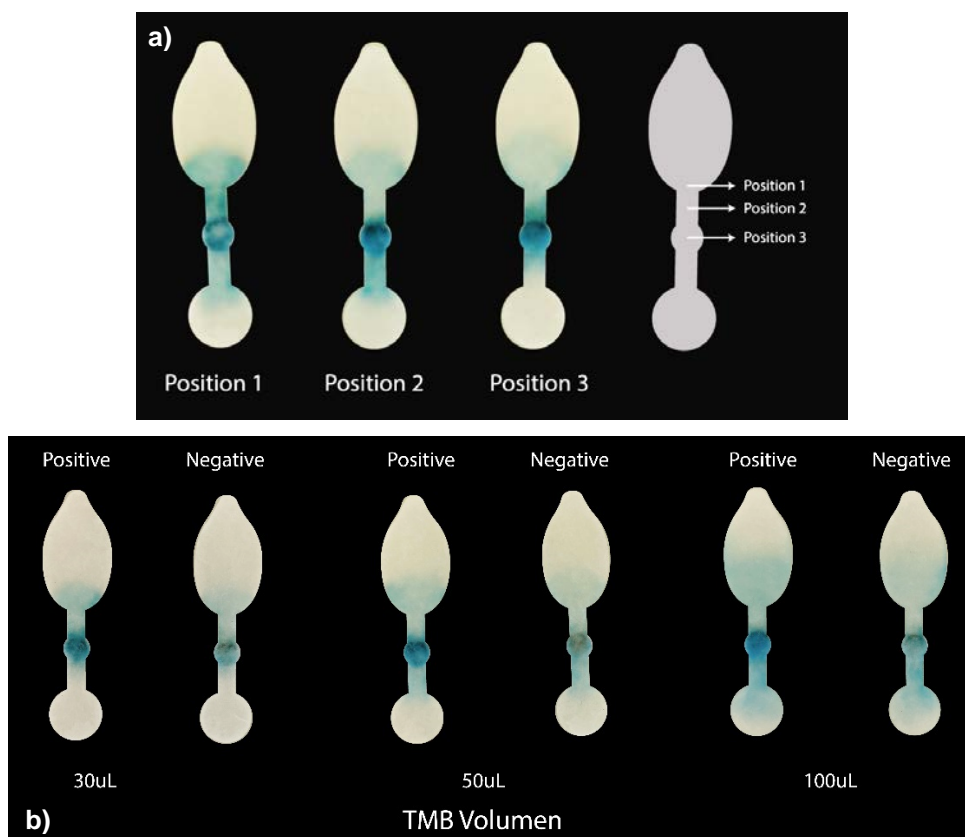


**Figure S5. Optimization of the concentration of MBs in the paper-based magneto-immunoassay.**

a) Colorimetric readouts (calculated using ImageJ) and b) S/N ratios obtained in the paper-based magneto-immunoassay for Pf-LDH concentrations ranging 12.5-50 ng·mL<sup>-1</sup>, using for immunocapture three amounts of MBs (10-20 µg per sample; Invitrogen MyOne Dynabeads).

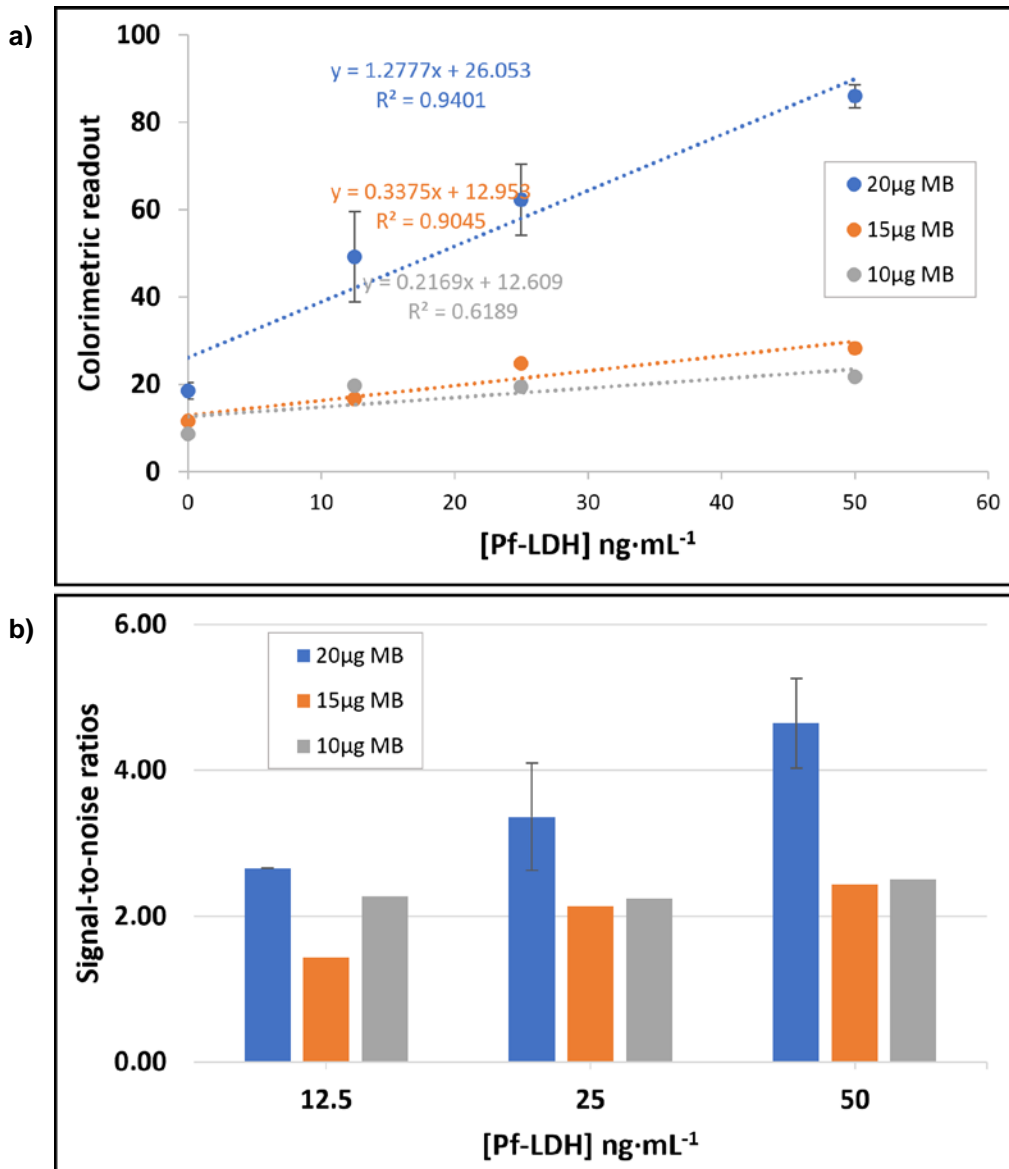


**Figure S6. Comparative performance of MBs from Invitrogen and GE Healthcare.**

Invitrogen Dynabeads, used in the previous sections, were compared to GE Healthcare SeraMag MBs which, according to the provider, display higher magnetic content. In our experiments, SeraMag MBs exhibited faster magnetic concentration than Dynabeads. However, they provided also higher background noise and lower signals for all the concentrations of Pf-LDH studied, providing significantly lower S/N. (a) Optical densities measured at 450 nm for the magneto-immunoassay carried in tubes and (b) colorimetric readouts registered for the paper-based magneto-immunoassay for increasing Pf-LDH concentrations (1.56-12.5 ng·mL<sup>-1</sup> and 3.13-50 ng·mL<sup>-1</sup>, respectively), when using alternatively the two types of MBs (GE Healthcare SeraMag MBs and Invitrogen Dynabeads, in both cases carboxy-modified and 1 µm in diameter MBs, modified with c-MAb).

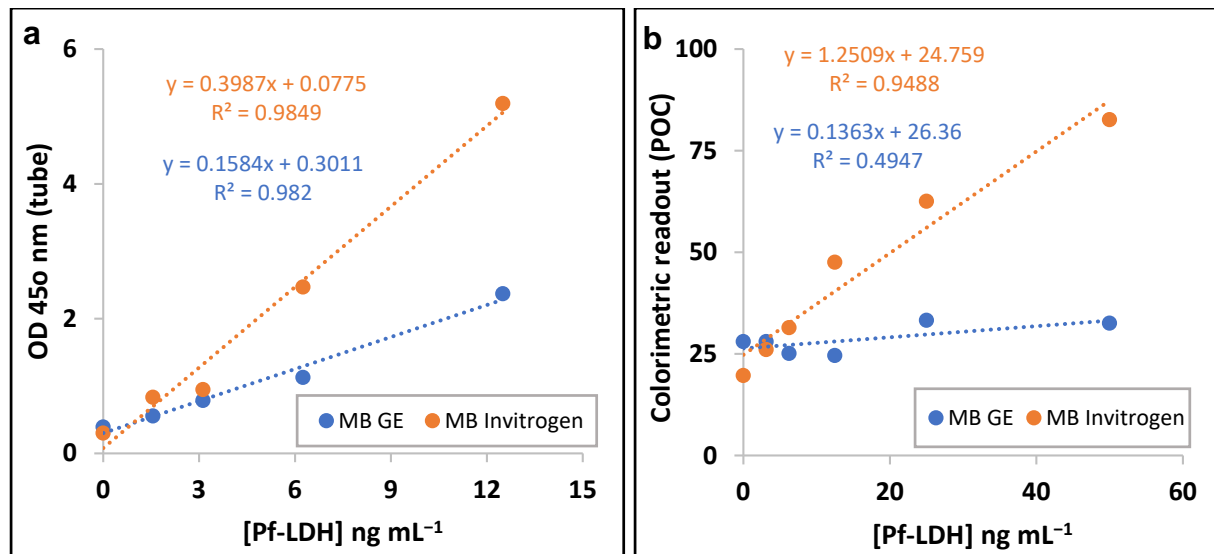


**Figure S7. Detection of Pf-LDH in PBST-BSA and blood using the POC device.**

Images obtained in four independent calibration experiments using the single-step magneto-immunoassay directly in the paper device to detect increasing concentrations of Pf-LDH in PBST-BSA or in lysed whole blood (diluted 1:10 and 1:100 with PBST-BSA). Each paper device was used only once. Accordingly, each image was obtained with a different paper device.

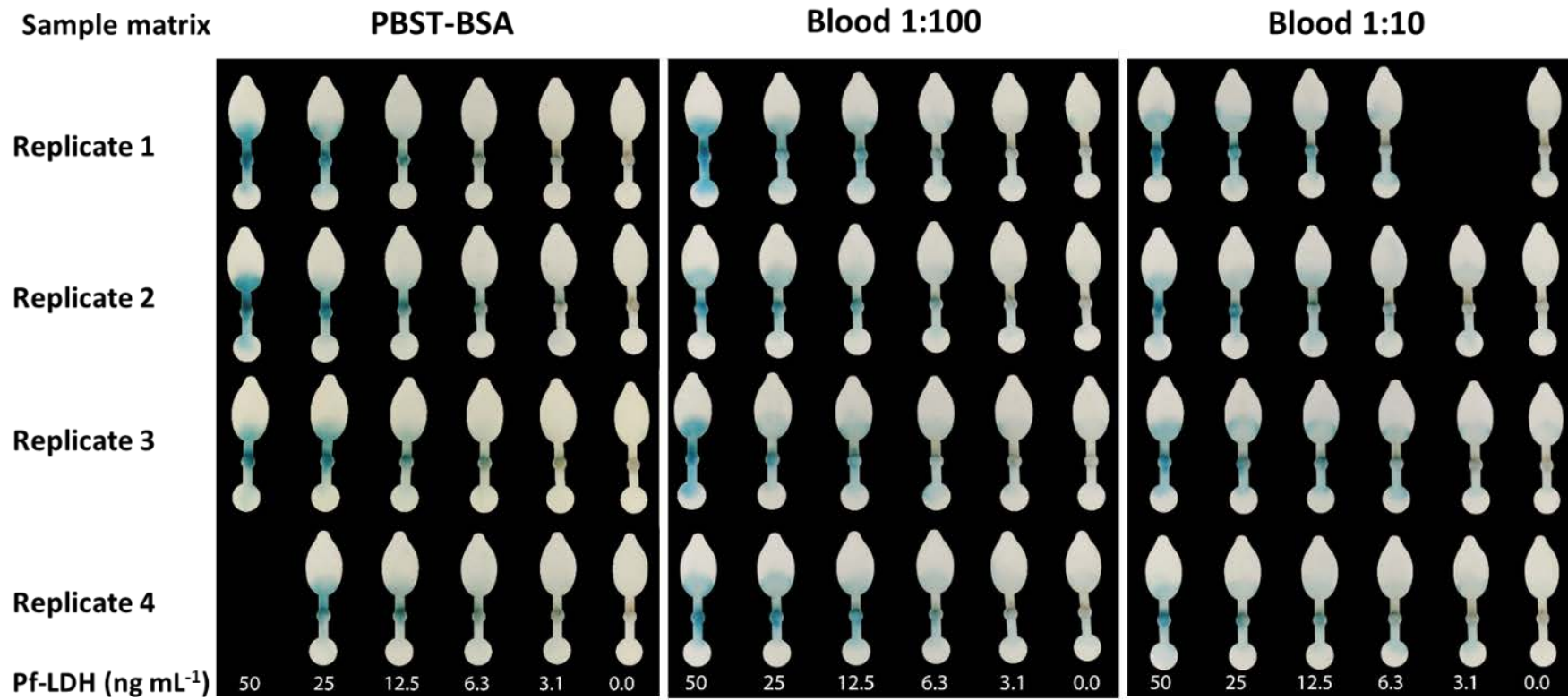


**Figure S8. Study of clinical samples using the  $\mu$ PAD.**

Nine whole blood samples obtained from malaria patients were analysed using the paper-based magneto-immunoassay. For this, samples were mixed 1:1 with lysis buffer, were incubated for 5 min and were diluted 1:10 and 1:100 with PBST-BSA. These lysed samples were then analysed using the paper-based magneto-immunoassay as detailed in the protocol in the main manuscript. Seven of the 9 samples were detected by the POC after a 1:10 dilution. Only samples P4 and P5, which corresponded to two submicroscopic malarias, were missed by the naked eye (one of the replicates was interpreted as a faint positive, but the other as negative). For samples diluted 1:100, only the highest parasitaemias could be detected (P3 and P9).

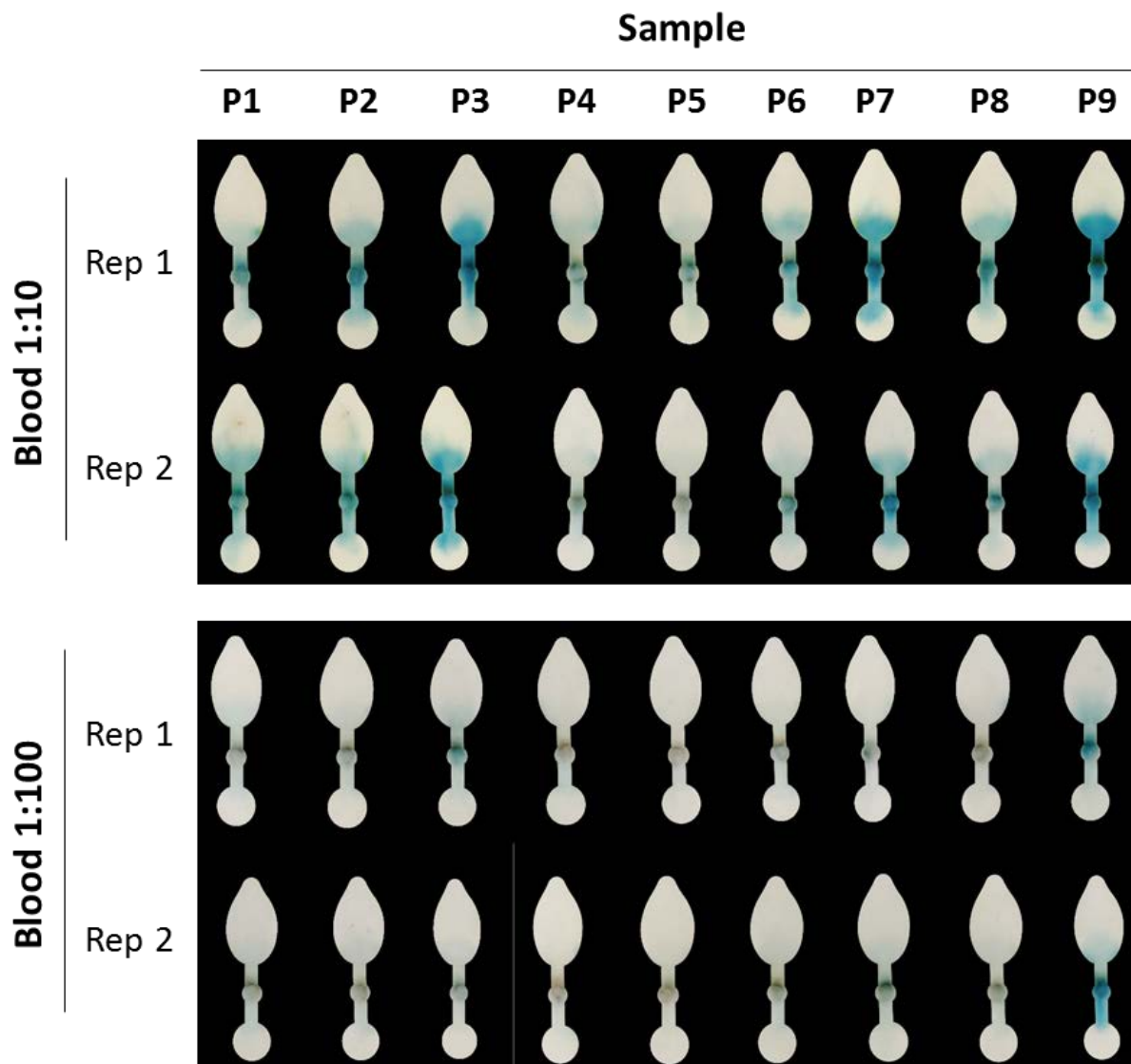


**Figure S9. Study of clinical samples using a commercial RDT.**

The nine clinical samples were analysed in parallel using a commercial RDT (SD BIOLINE Malaria Antigen Pf/Pan RDT, ABBOT - formerly Alere - ref. 5FK60), following the instructions provided by the supplier. This RDT displays a control line and two test lines for multiplexed detection of *Plasmodium falciparum* HRP2 (Pf-HRP2) and Pan *Plasmodium* LDH (pLDH).

Seven of the 9 samples were positive for Pf-HRP2 (P2, P3, P4, P6, P7, P8 and P9), P1 displayed a faint positive, and P5 was clearly negative for Pf-HRP2. In contrast, 7 of the samples were negative for pLDH and only two of the samples, P3 and P9, were faintly positive for pLDH.

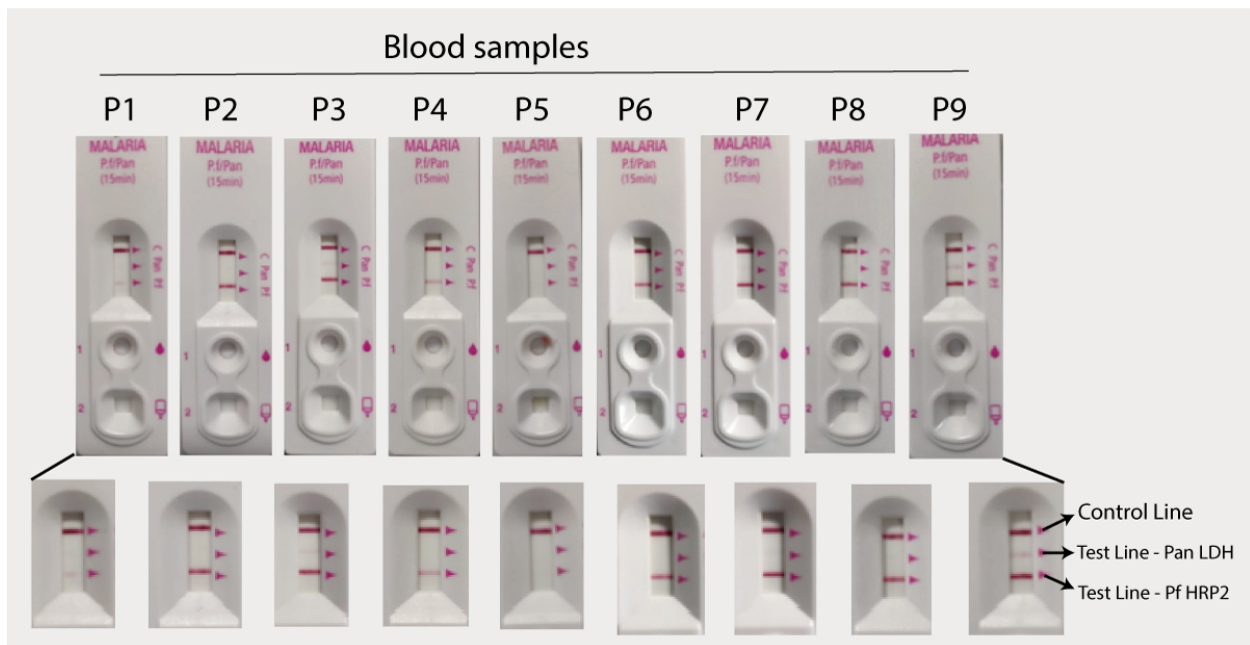


### **Figure S10. External evaluation of semiquantitative naked eye colour interpretation**

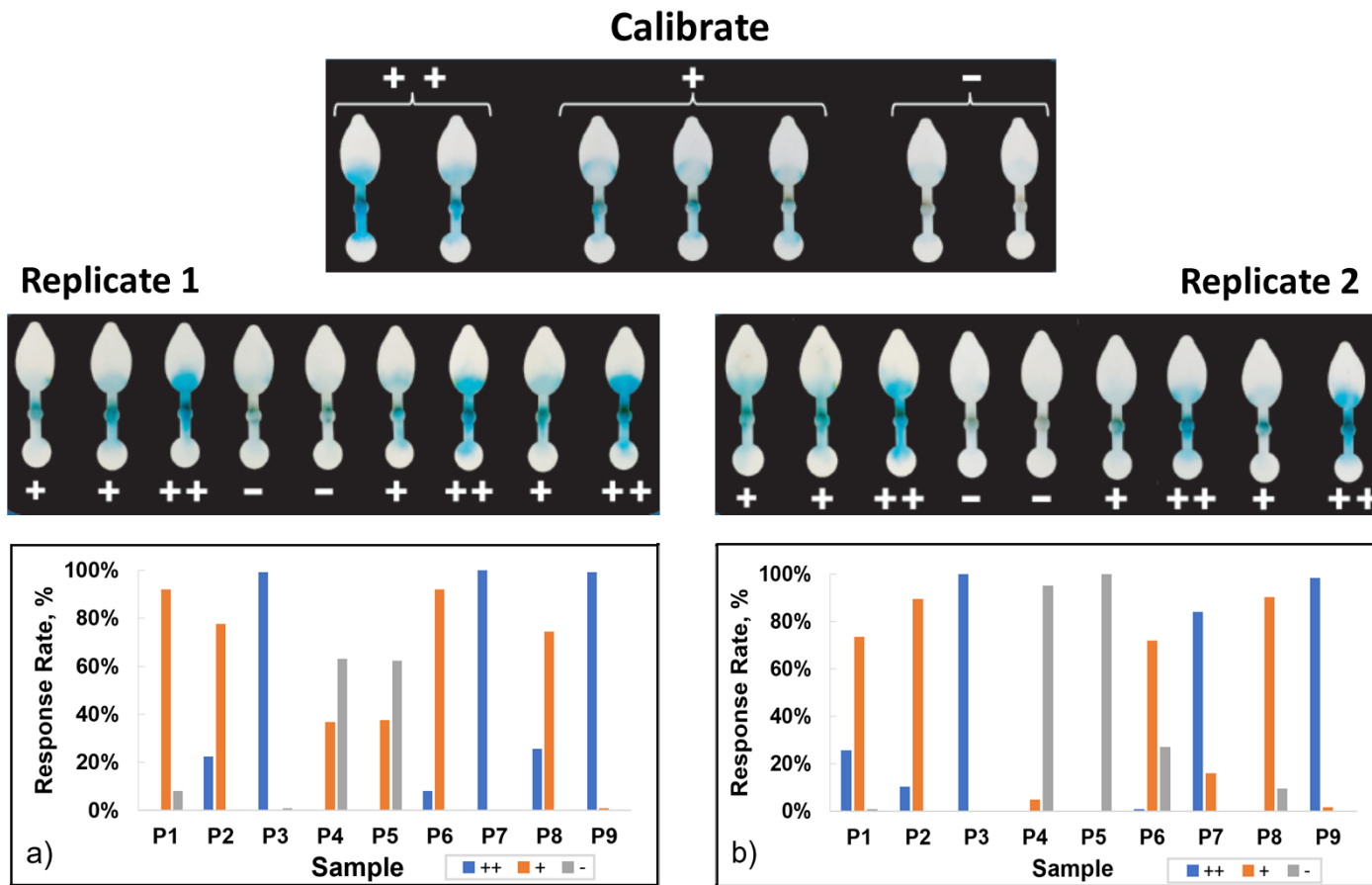
Three questionnaires were produced to study the accuracy of  $\mu$ PAD result interpretation by users not familiar with the technology employed here. The forms were created using the EU Survey Tool for a correct data management in accordance with European legislation (EU) 2016/679. They were circulated in the social media and spread word of mouth among personal contacts and Vall d'Hebron Hospital personnel.

Each form included pictures of a calibrate and results obtained for a set of clinical samples (2 replicates each, but shown to users as independent samples). Users had to interpret colour intensity in the samples in a semi quantitative way, according to the corresponding colour reference scale of the calibrate.

The results obtained for each form are summarized next where, for each questionnaire, we show the pictures of the calibrate and samples that were offered to the volunteers. Result interpretation included here in the pictures of samples corresponds to the concentration of Pf-LDH obtained by ELISA and was not facilitated to users in the questionnaires. The graphs summarize the % of responses that attributed each quantitative category to each sample.

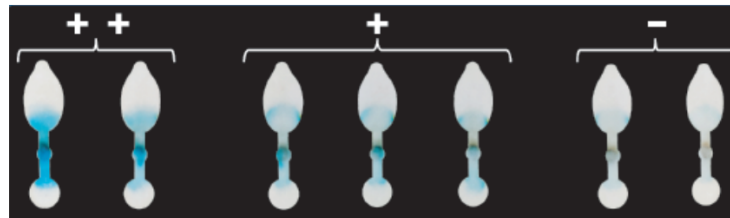
According to the results, parameters such as user sex, age and gender had no effect on result interpretation. In the same way, there were no statistical differences between the responses of individuals with and without previous experience in the performance and interpretation of rapid diagnostic tests, or between professionals working in the health sector and the rest. In contrast, result interpretation accuracy was slightly higher among individuals having responded using a computer screen, compared to those having used the screen of a mobile phone.

The **first form** used a reference colour code that included three categories (++, +, -) and the audience was asked to classify independently the two replicates of the nine malaria samples of Figure S-8 (blood 1:10). This form was answered by 136 individuals. As it can be observed, samples were interpreted with a high level of agreement, except for the first replicate of samples P4 and P5, which were close to the device limit of detection. Nevertheless, answers achieved a success rates of 84% and 89% for the first and second replicate sets, respectively.

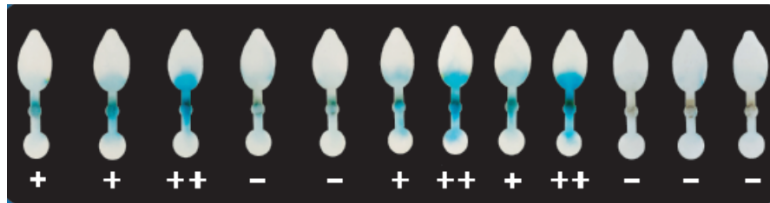


The **second form** used the same reference scale as the first form (++ , + , -), but three negative samples were included after the images of the samples positive for malaria. This made that part of the interviewees (n=270) interpreted the first replicates of samples P4 and P5 and positives, with average success rates of 80% and 90% for the first and second replicate sets, respectively.

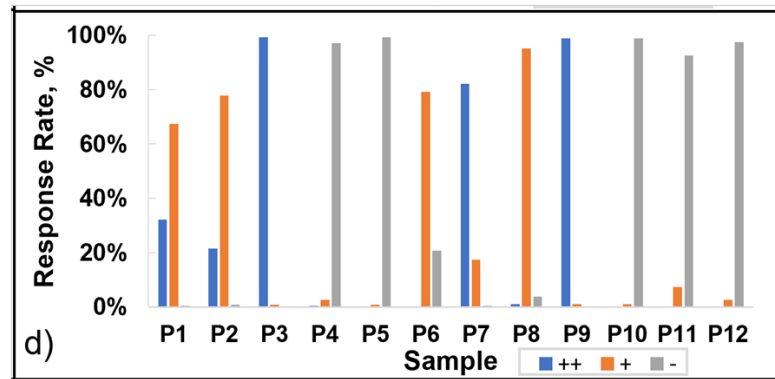
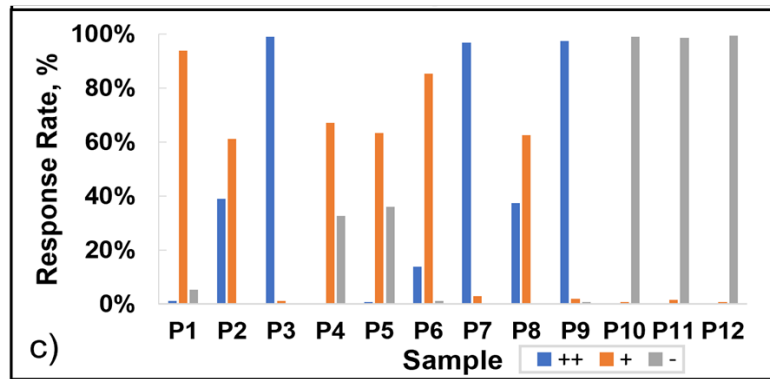
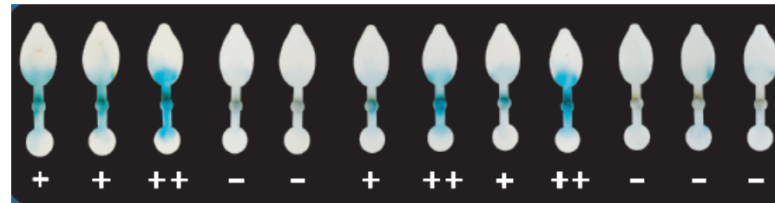
### Calibrate



### Replicate 1



### Replicate 2



Finally, in the **third form**, a new category was added to the reference scale (+++, ++, +, -) in an attempt to obtain a semi quantitative system (for upper-, middle- and low-parasitaemia malaria positive samples). In this last form, 9 positive and 3 negative outcomes were given to the public, whose replicates were reassembled randomly in the two pictures of samples. Contrary to the first two forms, in this case instructions were given to facilitate result interpretation. The 77 users who answered had success rates of 91% and 82% in the first and second replicate sets, respectively.

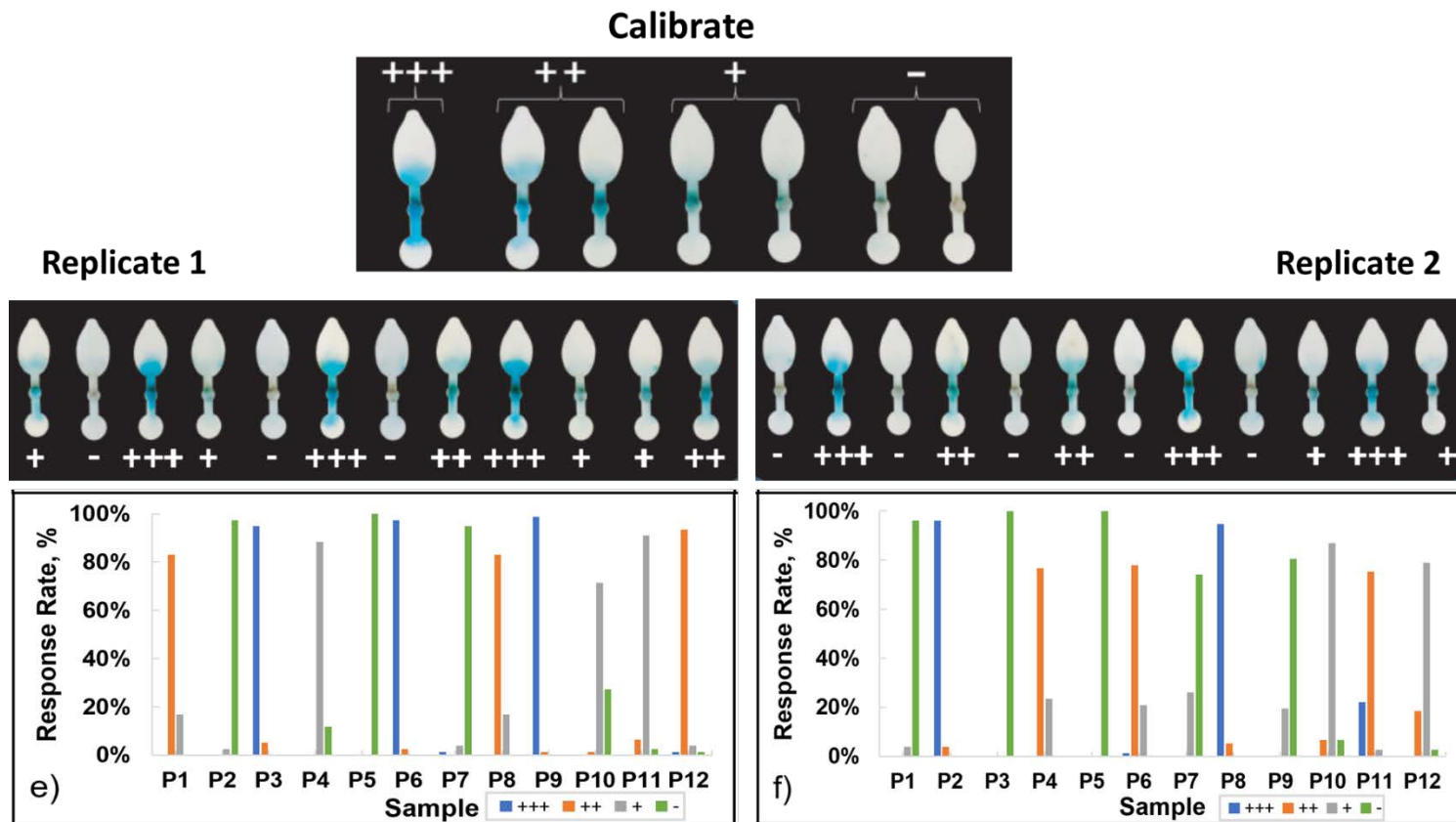


**Table S1. Summary of the results obtained in the analysis of clinical samples from malaria patients.**

Blood samples from 9 patients infected with *P. falciparum* were analysed by microscopy, ELISA, a commercial RDT (detecting both biomarkers Pf-HRP2 and Pan LDH), and the  $\mu$ PAD developed in this work. Visual interpretation of the  $\mu$ PAD readout was made independently on the two replicates obtained per sample (Figure S-8; blood 1:10), taking as the reference the calibrate in Figure 4a in the main manuscript. The concentration of Pf-LDH was calculated by interpolation of the images' analysis in the calibrate obtained for spiked blood (1:10; Figure 4c).

Sample	Microscopy	ELISA	Commercial RDT		$\mu$ PAD		
	(% parasitaemia)	(ng mL <sup>-1</sup> )	Pf-HRP	Pan LDH	Rep 1	Rep 2	ng mL <sup>-1</sup>
P1	+ (0.3)	+ (91)	-/+	-	+	+	145
P2	+ (0.6)	+ (240)	+	-	+	++	177
P3	+ (0.3)	+ (649)	+	+	++	++	750
P4	-	+ (30)	+	-	+/-	-	36
P5	-	+ (91)	-	-	-	-	19
P6	+ (0.2)	+ (106)	+	-	+	+	112
P7	+ (0.1)	+ (570)	+	-	++	++	274
P8	+ (0.8)	+ (316)	+	-	+	+	65
P9	+ (0.8)	+ (2132)	+	+	++	++	2212

**Table S2. Summary of the results obtained for the control blood samples.**

Blood samples from 8 healthy patients were analysed by ELISA, a commercial RDT (detecting both biomarkers Pf-HRP2 and Pan LDH), and the  $\mu$ PAD developed in this work. Visual interpretation of the  $\mu$ PAD readout was made independently on the two replicates obtained per sample (blood 1:10), taking as the reference the calibrate in Figure 4a in the main manuscript.

Sample	ELISA	Comercial RDT		$\mu$ PAD
		Pf-HRP	Pan LDH	
C1	-	-	-	-
C2	-	-	-	-
C3	-	-	-	-
C4	-	-	-	-
C5	-	-	-	-
C6	-	-	-	-
C7	-	-	-	-
C8	-	-	-	-

**Table S3. Estimate of the production cost of the retail-purchased reagents of  $\mu$ PAD** (indirect and personnel costs not included).

Reagent	Amount / test	Price / stock unit	Price / test
MBs	20 $\mu$ g	144.40 € / 20 mg	0.144
c-MAb	0.5 $\mu$ g	165.60 € / 1 mg	0.0828
bd-MAb	8.25 ng	165.60 € / 1 mg	0.0014
Poly-HRP	5.5 ng	215.1 € / 0.5 mg (0.5 mg·mL <sup>-1</sup> )	0.0024
TMB	50 $\mu$ L	237 € / 400 mL (4x100mL)	0.0296
Sensors (Standard 17)	1	8.72 € / sheet = 114 chips	0.0765
Absorbent pads (CF5)	1	7.99 € / sheet = 72 absorbent pads	0.1110
<b>Total / test</b>			<b>0.4480</b>

## Bibliography

1. Ruiz-Vega, G.; Arias-Alpizar, K.; de la Serna, E.; Borgheti-Cardoso, L. N.; Sulleiro, E.; Molina, I.; Fernández-Busquets, X.; Sánchez-Montalvá, A.; del Campo, F. J.; Baldrich, E. Electrochemical POC Device for Fast Malaria Quantitative Diagnosis in Whole Blood by Using Magnetic Beads, Poly-HRP and Microfluidic Paper Electrodes. *Biosens. Bioelectron.* **2020**, *150*, 111925, doi:10.1016/j.bios.2019.111925.
2. Arias-Alpizar, K.; Sánchez-Cano, A.; Prat-Trunas, J.; de la Serna, E.; Alonso, O.; Sulleiro, E.; Sánchez-Montalvá, A.; Diéguez, A.; Baldrich, E. Malaria quantitative POC testing using magnetic particles, a paper microfluidic device and a hand-held fluorescence reader. *Biosens. Bioelectron.* **2022**, *215*, 114513, doi.org/10.1016/j.bios.2022.114513.